Structure and spectroscopy of U^{4+} defects in Cs_2ZrCl_6: *Ab initio* theoretical studies on the $5f^2$ and $5f^16d^1$ manifolds

Zoila Barandiarán[a] and Luis Seijo
Departamento de Química, C-XIV and Instituto Universitario de Ciencia de Materiales Nicolás Cabrera, Universidad Autónoma de Madrid, 28049 Madrid, Spain

(Received 24 September 2002; accepted 28 January 2003)

The *ab initio* model potential embedded cluster method, which combines the explicit treatment of quantum-mechanical embedding effects with electron correlation and spin–orbit coupling, has been applied to the calculation of the U–Cl equilibrium distances, totally symmetric vibrational frequencies, and $5f^2 \rightarrow 5f^2$, $5f^2 \rightarrow 5f^16d^1$ electronic transitions of the $(UCl_6)^{2-}$ defect cluster in the Cs_2ZrCl_6 host crystal. The $5f^2 \rightarrow 5f^2$ absorption spectrum of U^{4+} in gas phase has also been calculated. Comparison of the $5f^2 \rightarrow 5f^2$ spectra in gas phase and in Cs_2ZrCl_6 with experiments is used for establishing the accuracy of the methods and understanding the origins of the discrepancies between theory and experiments; the agreement between the calculated and experimental values are very satisfactory. The energies of the crystal levels of the $5f^16d(t_{2g})^1$ and $5f^16d(e_g)^1$ manifolds are predicted to be 31 100–51 000 and 67 300–85 500 cm^{-1} above the ground state, respectively. The lowest electric dipole allowed zero-phonon absorption from the $5f^2$ ground state, $1A_{1g} \rightarrow 1T_{1u}$, is calculated to be at 32 500 cm^{-1}, whereas the highest electric dipole allowed zero-phonon emission from the first $5f^16d(t_{2g})^1$ excited state, which is found to be $1E_u \rightarrow 1T_{1g}$, is calculated to be at 30 200 cm^{-1}; this means that both of them should be observable before the sharp cutoff of the Cs_2ZrCl_6 host with a large gap of 2300 cm^{-1} between the zero-phonon absorption and emission lines. The combination of experimental spectroscopic data on $Cs_2ZrCl_6:U^{4+}$, $Cs_2ZrCl_6:UO_2^{2+}$, and $Cs_2UO_2Cl_4$, with the calculated energy levels of the $Cs_2ZrCl_6:U^{4+}$ $5f^16d(t_{2g})^1$ manifold allows to discuss new possible mechanisms which could explain the observed green to blue upconversion emission of $Cs_2ZrCl_6:U^{4+}$ crystals contaminated with UO_2^{2+}. Altogether, the results in this paper demonstrate the potentiality of the wave function based methods of solid-state quantum chemistry for complementing experimental techniques in the study of actinide systems like U^{4+}-doped Cs_2ZrCl_6 where hundreds of excited states are involved and their electronic structure is determined by strong spin–orbit and electron correlation interactions. © *2003 American Institute of Physics.* [DOI: 10.1063/1.1561853]

I. INTRODUCTION

Doping impurity ions in a crystal is a common way to produce new spectral signals in the optical window of the host, which results in new optical properties of basic and technological interest. Upconversion luminescence is a good example of this where the absorption of low energy photons by the impurity, followed by different energy transfer mechanisms involving a number of metastable electronic states, leads to emission of higher energy light, which ultimately may serve to different technological purposes. Upconversion luminescence has been widely investigated among lanthanide ions in glasses and crystals, but an increasing number of reports involve other impurities: $4d$ and $5d$ transition metal ions,[1] mixed transition metal and lanthanide ions,[2] and actinide ions.[3–9] Even though a variety of photon upconversion mechanisms have been described,[2] two very general mechanisms usually occur which involve either sequential excitation of a single ion or energy transfer between two ions which have been excited.[10] Whatever the mechanism is, high energy excited states are involved which, in the case of actinide impurities, include not only high energy $5f^n$ states but also $5f^{n-1}6d^1$ levels of the impurity ions. Actually, the relative energies of the $5f^n$ and $5f^{n-1}6d^1$ manifolds also determine other important spectroscopic properties, such as the occurrence or not of efficient $5f^{n-1}6d^1 \rightarrow 5f^n$ luminescence, which is very important in the field of ultraviolet (UV) solid-state lasers.[11] In this context, the capabilities of experimental spectroscopic methods and of *ab initio* solid-state quantum chemistry should be combined together: Spectroscopic techniques can locate and identify the $5f^n$ manifold very precisely, in general, whereas the prediction and/or assignment of $5f^n$–$5f^{n-1}6d^1$ interconfigurational transitions is much more limited and should benefit from the capabilities of sophisticated *ab initio* solid-state quantum chemistry calculations. Very recently, Kirikova *et al.*[11] have pointed out the scarce number of reports on $5f^{n-1}6d^1 \rightarrow 5f^n$ luminescence, on the one hand, and the lack of theoretical calculations regarding the energy position of the levels of the $5f^{n-1}6d^1$ electronic configuration of tetravalent actinides in crystal hosts, on the other hand, as circumstances which prevent any predictions regarding the spectra from interconfigurational transitions for actinide ions in different hosts.[11]

[a]Electronic mail: zoila.barandiaran@uam.es

In the case of U^{4+}-doped Cs_2ZrCl_6 single crystals, neither the local structure nor the energies of the $5f^16d^1$ manifold are known. Furthermore, very different interpretations of the observed green to blue upconversion emission in $Cs_2ZrCl_6:U^{4+}$ samples at room temperture, have been reported.[6,12] In effect, relatively strong blue upconversion emission has been detected in $Cs_2ZrCl_6:U^{4+}$ samples under green light excitation.[6,12] This upconversion emission has been interpreted by Xu *et al.*[6] as a two-photon absorption process involving two metastable $5f^2$ excited levels and a so called "virtual" level of U^{4+}: A first photon in the green ($19\,436\ cm^{-1}$) excites the impurity into a level related to the $5f^2\ {}^3P_1$ of the free ion; nonradiative decay to a low lying level ($\sim 5000\ cm^{-1}$ above the ground state) related to $^3F_2$ is expected to occur from where the second $19\,436\ cm^{-1}$ photon is absorbed. This excited state absorption ends in a virtual level and is followed by nonradiative relaxation down to several $5f^2$ states which emit upconverted light in the blue (five band centers are found from 19 800 to 20 970 cm^{-1}).[6] The virtual level invoked as one of the intermediate excited states in the process has not been identified, even though the absorption spectra of $Cs_2ZrCl_6:U^{4+}$, Cs_2UCl_6, and other crystals containing the $(UCl_6)^{2-}$ complex,[13,14] measured at low temperature, show that the $5f^2$ manifold of states extends up to $24\,800\ cm^{-1}$ (with only one exception: The $^1S_0$ level, which is predicted to be at about $41\,700\ cm^{-1}$, too high in energy to be playing any significant role in the upconversion mechanism), which suggests that the virtual level in the upconversion mechanism proposed by Xu *et al.*[6] could be one of the highest in energy in the $5f^2$ manifold. Tanner *et al.*[12] have interpreted the green to blue upconversion emission very differently: First, they claim that the preparative procedures followed by themselves[12] and by Xu *et al.*[6] for the incorporation of U into the Zr^{4+} sites of Cs_2ZrCl_6 can result in occupation by both U^{4+} and UO_2^{2+} ions, and, second, they conclude after referring to the 300 K spectra of $Cs_2ZrCl_6:UO_2^{2+}$ and $Cs_2UO_2Cl_4$ that the reported blue upconversion of U^{4+} in Cs_2ZrCl_6 does in fact correspond to luminescence of the uranyl ion, UO_2^{2+}.[12]

The experimental information we have summarized makes the $Cs_2ZrCl_6:U^{4+}$ crystal an interesting system to be studied theoretically. Consequently, we have calculated the potential energy surfaces of all electronic states of $5f^2$ and $5f^16d^1$ main configurations using the *ab initio* model potential (AIMP) embedded-cluster method.[15,16] The results of the calculations are the U–Cl equilibrium distance and totally symmetric vibrational frequency, $\overline{\nu}_{a_{1g}}$, of the octahedral $(UCl_6)^{2-}$ embedded unit, for all electronic states, and the $5f^2\rightarrow 5f^2$ and $5f^2\rightarrow 5f^16d^1$ electronic transition energies. The analysis of the spin–orbit wave functions of all the embedded $(UCl_6)^{2-}$ electronic states reveals the extent of spin–orbit coupling among the spin-free $(UCl_6)^{2-}$ cluster wave functions; this analysis often leads to establish a certain parentage to U^{4+} free ion levels, but this is not always possible and very large mixings are present, given the large and simultaneous effects of spin–orbit, crystal field splittings and bonding interactions that occur in this material and are incorporated by the methods used. The calculated U–Cl equilibrium distances are extremely close among the electronic states belonging to the three following superconfigurations: 2.605 ± 0.003 Å for $5f^2$, 2.571 ± 0.004 Å for $5f^16d(t_{2g})^1$, and 2.642 ± 0.004 Å for $5f^16d(e_g)^1$, in agreement to what has been found in similar systems.[17–19] The deviation of the $5f^2\rightarrow 5f^2$ transition energies from experiment are found to grow with energy, the largest error being $\sim 2000\ cm^{-1}$. The energies of the lowest states in the $5f^16d(t_{2g})^1$ and $5f^16d(e_g)^1$ manifolds are calculated to be 31 100 and $67\,300\ cm^{-1}$ above the $5f^2\ 1A_{1g}$ ground state, respectively. The lowest symmetry allowed electric dipole zero-phonon absorption from the $5f^2$ ground state, $1A_{1g}\rightarrow 1T_{1u}$, and the highest symmetry allowed electric dipole zero-phonon emission from the first $5f^16d(t_{2g})^1$ excited state, which is found to be $1E_u\rightarrow 1T_{1g}$, are calculated to be at 32 500 and $30\,200\ cm^{-1}$, respectively, which means that they should be observable before the sharp cutoff of the Cs_2ZrCl_6 host at $37\,000\ cm^{-1}$,[20] with a large gap of $2300\ cm^{-1}$ between the zero-phonon lines of the absorption and emission spectra.

The results of our calculations give some insight into the discussion on the green to blue upconversion. They suggest that $5f^16d^1$ excited electronic states of the embedded $(UCl_6)^{2-}$ cluster are involved in the upconversion mechanism in a way that supports part of the interpretation of Xu *et al.*[6] and the interpretation of Tanner *et al.*[12] In effect, the first green excitation of $(UCl_6)^{2-}$ could be followed by a nonradiative decay as proposed by Xu *et al.*,[6] although shorter than the one they suggest, due to the fact that several $5f^2$ electronic states of high spin-singlet character lie above $14\,800\ cm^{-1}$ and can be expected to be stable enough so as to become origins of a second green excitation, which would end in a $5f^16d^1$ state and would be, in consequence, parity allowed. According to this, the virtual state mentioned by Xu *et al.*[6] would be of a $5f^16d^1$ nature. Now, nonradiative decay from this state to high energy U^{4+} $5f^2$ states, followed by blue light emission would complete the interpretation of Xu *et al.*[6] Alternatively or simultaneously, energy transfer from the proposed $5f^16d^1$ state of U^{4+} to UO_2^{2+} could occur in contaminated $Cs_2ZrCl_6:U^{4+}$ crystals, which would be followed by the UO_2^{2+} emission claimed by Tanner *et al.*[12] According to this, the mechanism for the complete or partial quenching of the U^{4+} blue emission due to UO_2^{2+} contamination[12,21] would be very similar to the one proposed by Laroche *et al.*[22] to interpret the blue to violet+UV upconversion of Ce^{3+} in Cs_2NaYCl_6 co-doped with Ce^{3+} and Pr^{3+}.

Our wave function and energy calculations cannot give a definite answer to the actual upconversion mechanism which accompanies $19\,436\ cm^{-1}$ green argon ion laser excitation, nor can they rule out U^{4+} or UO_2^{2+} ions as luminescent centers. Rather, they can provide the energy levels of the $5f^16d^1$ manifold with high accuracy, which makes it possible to consider the efficient dipole allowed $5f^2$–$5f^16d^1$ electronic transitions in the discussion of U^{4+}/UO_2^{2+} green to blue upconversion. Probably, experimental studies on U^{4+} and UO_2^{2+} co-doped Cs_2ZrCl_6 samples like those in Ref. 22, which take into account the location of the U^{4+} $5f^16d^1$ levels reported here, could further clarify these problems.

The paper is organized as follows: The methods used to treat host effects, electron correlation, and scalar and spin-dependent relativistic effects are summarized in Sec. II, where the details of the calculations are also given. The results of the calculated absorption spectrum of U^{4+} in gas phase are presented and discussed in Sec. III. The calculated local structure, and $5f^2-5f^2$ and $5f^2-5f^16d^1$ absorption spectra are presented and discussed in Sec. IV, and the upconversion mechanism which is suggested by our results is discussed in Sec. V. The conclusions of this work are given in Sec. VI.

II. METHOD AND DETAILS OF THE CALCULATIONS

A. The Cs_2ZrCl_6 embedding potential

The U^{4+} impurities substitute for Zr^{4+} ions of the Cs_2ZrCl_6 host crystal, which creates octahedral $(UCl_6)^{2-}$ defect clusters. The spectral properties of the $Cs_2ZrCl_6:U^{4+}$ material mentioned in the Introduction are largely attributed to electronic states strongly localized in this unit. Yet, the influence of the surrounding crystal beyond the chlorine first neighbors is known to be important in this type of materials.[15] Thus, a quantum-mechanical method which partitions the crystal electronic structure accordingly, such as the *ab initio* model potential (AIMP) embedded cluster method,[15,16] must be used to account for host effects and to focus the highest methodological and computational effort on the $(UCl_6)^{2-}$ complex. Readers interested in the details of the AIMP embedded cluster method, the works which prove its accuracy as an embedding technique, and the results obtained in a number of applications to the calculation of the local structure and spectroscopy of transition metal ion impurities in ionic hosts (at ambient and high pressures) are referred to the review chapter of Ref. 15. More recent applications, which further support the accuracy of the embedding, include high pressure modeling in $Cs_2NaYCl_6:V^{3+}$ (Ref. 23) and studies of the structure and spectroscopy of actinide impurities in ionic hosts.[17–19] Here, we only summarize the embedding method whose results can be considered essentially free from errors due to inadequate representations of host effects beyond first neighbors.

The embedding potentials which represent the Cs_2ZrCl_6 ions external to the $(UCl_6)^{2-}$ cluster in the $Cs_2ZrCl_6:(UCl_6)^{2-}$ calculations presented here were obtained in a previous study of the structure and spectroscopy of Pa^{4+} defects in Cs_2ZrCl_6.[17] They accurately reproduce the quantum-mechanical interactions between (frozen) Hartree–Fock descriptions of the external crystal ions (e.g., Cs^+, Zr^{4+}, and Cl^- in Cs_2ZrCl_6) and the (multiconfigurational) wave functions associated with the point defect cluster $(UCl_6)^{2-}$. They include (i) a long-range Coulomb term, which in ionic crystals is the corresponding Madelung potential, (ii) a short-range Coulomb term, which corrects the latter taking into account that the lattice ions are not point charges, but charge densities associated with Hartree–Fock wave functions, (iii) an exchange term, which stems from the fact that the generalized antisymmetric product of the cluster and the external ion wave functions fulfil the first principles requirement of antisymmetry with respect to interchange of electrons between the cluster and lattice group functions, and (iv) a projection term, which guarantees that the defect cluster and external ion wave functions are built using linearly independent sets of orbitals; this term actually prevents variational collapse of the cluster wave functions on the lattice ions. The embedding potential data can be found in Ref. 24.

B. The *sfss* relativistic Hamiltonian: Electron correlation and spin–orbit coupling

The chemical bonds that the U^{4+} impurities establish with the surroundings are expected to be confined within the $(UCl_6)^{2-}$ cluster, whose large manifold of electronic states corresponds to a multireference $5f^2$, $5f^16d^1$ open-shell system. Consequently, wave function based molecular quantum-chemistry methods which include nondynamic and dynamic electron correlation, and which have been developed and proved to be accurate for the study of the chemical bond and spectroscopy of molecules in gas phase, are a good option, provided that the embedding potentials are added to the molecular cluster Hamiltonian. Relativistic effects including spin–orbit coupling are equally important and are compulsory, which adds up to the methodological challenges posed by these systems. Given the large number of valence electrons to be correlated (48 from all six Cl and 10 from U) the simultaneous treatment of electron correlation and spin–orbit coupling through multireference spin–orbit configuration interaction (CI) calculations is very much restricted. Here, we treat both effects by means of a two-step procedure based on the spin-free state shifted (sfss) relativistic Hamiltonian,[25] which involves an approximate decoupling of electron correlation and spin–orbit coupling effects. In a first step of spin-free Hamiltonian calculations, scalar relativistic effects and electron correlation are dealt with at the highest methodological level possible. The electron correlation effects on the calculated transition energies are then transported by the sfss operator to the second step where spin–orbit CI calculations are performed in a smaller configurational space. This strategy is possible since electron correlation and spin–orbit effects have been found to be largely decoupled in similar systems like $MgO:Ni^{2+}$,[25] $Cs_2NaYCl_6:Ce^{3+}$,[26] $Cs_2ZrCl_6:Pa^{4+}$,[17] or $Cs_2NaYCl_6:U^{3+}$.[19] The details of the two-step calculations are given next. See also Refs. 15, 17, and 19.

1. Spin-free Hamiltonian calculations

The $(UCl_6)^{2-}$ wave functions and energies corresponding to the spin-free embedded cluster Hamiltonian were calculated using an extension of the second-order multiconfigurational perturbation method CASPT2,[27,28] the multistate CASPT2 method.[29] This extension, based on the multipartitioning quasidegenerate perturbation theory,[30] is particularly useful for the calculation of the potential energy surfaces of the $(UCl_6)^{2-}$ excited states, since many electronic states of the same symmetry are close together in energy so that strong interactions and even avoided crossings should be expected. In this context, the choice of active space, basis set of U, and dynamic correlation appropriate for studies of $5f^n$ and $5f^{n-1}6d^1$ manifolds of actinide ions in halide crystals

have been recently investigated on $Cs_2NaYCl_6:U^{3+}$.[19] Analogous choices have been adopted here and are described next. State average complete active space self-consistent field[31] (SA-CASSCF) calculations were performed for all electronic states of the 19 spin and octahedral irreducible representations ($^{3,1}\Gamma_{g,u}$; $\Gamma = A_1$, A_2, E, T_1, T_2, except $^3A_{1g}$) by generating all possible configurations where two open-shell electrons occupy the 12 molecular orbitals of main character U $5f$ (a_{2u}, t_{2u}, t_{1u}) and U $6d$ (t_{2g}, e_g). The orbital optimization was done on eight separate state average calculations: 4 of the $5f^2$ configurations, $\langle {}^3A_{2g}, {}^3E_g\rangle$, $\langle {}^3T_{1g}, {}^3T_{2g}\rangle$, $\langle {}^1A_{1g}, {}^1A_{2g}, {}^1E_g\rangle$, $\langle {}^1T_{1g}, {}^1T_{2g}\rangle$, and 4 of the $5f^16d^1$ configurations, $\langle {}^3A_{1u}, {}^3A_{2u}, {}^3E_u\rangle$, $\langle {}^3T_{1u}, {}^3T_{2u}\rangle$, $\langle {}^1A_{1u}, {}^1A_{2u}, {}^1E_u\rangle$, $\langle {}^1T_{1u}, {}^1T_{2u}\rangle$, where all the states of the indicated irreducible representation have been averaged in each case. The results of these multiconfigurational calculations will be referred to as CASSCF($5f$,$6d$). These manifolds of wave functions and energies can be labeled as $5f^{2-3,1}\Gamma_g$ and $5f^16d^{1-3,1}\Gamma_u$. As mentioned above, dynamic correlation energy was calculated for all $^{3,1}\Gamma_g$ and $^{3,1}\Gamma_u$ electronic states through multistate second-order perturbation theory (MS-CASPT2)[29,30] using the $5f^{2-3,1}\Gamma_g$ or the $5f^16d^{1-3,1}\Gamma_u$ CASSCF($5f$,$6d$) wave functions as the multidimensional reference space.[19] Following the conclusions of the study on $Cs_2NaYCl_6:U^{3+}$[19] referred above, 58 valence electrons were correlated which in the multidimensional reference occupy the molecular orbitals of main character U $6s$, $6p$, $5f$, $6d$ and Cl $3s$, $3p$. This type of calculations will be referred to as MS-CASPT2(Cl48,U10). It should be mentioned that the intermediate CASPT2 calculations revealed large and uniform weights ($>60\%$) of the zeroth-order reference in all states calculated at all distances and showed no signs of problems of intruder states, nor large contributions to the first-order wave function nor to the second-order energy correction which would indicate inadequacies on the choice of the complete active space used. Also, the MS-CASPT2(Cl48,U10) potential energy surfaces were found to be continuous functions of the U–Cl distance. All the spin-free calculations have been done using the relativistic core AIMPs and valence basis sets that are described next.

Relativistic effective core potentials corresponding to the *ab initio* model potential method (AIMP) have been published for the [Kr,$4d$]-core of the lanthanide elements and for the [Xe,$4f$,$5d$]-core of the actinide elements,[32] based on atomic Cowan–Griffin–Wood–Boring calculations,[33,34] together with optimized Gaussian valence basis sets and Wood–Boring spin–orbit operators.[32] These core sizes are known to be reasonable in quantum chemistry as long as energy differences between states of configurations with different f orbital occupation are not involved;[35] this has been shown to be a shortcoming in the calculation of $4f \rightarrow 5d/5f \rightarrow 6d$ transitions in L/An doped ions.[18] The transferability of frozen core potentials of neutral lanthanide and actinide elements to $4f/5f$ and $5d/6d$ states of their $3+$ and $4+$ ions has been investigated[18] and it has been found that a good description of the orbital spin–orbit coupling constants ζ_{4f}/ζ_{5f} and ζ_{5d}/ζ_{6d} of the Ln^{3+}/An^{4+} ions and of the $4f \rightarrow 5d/5f \rightarrow 6d$ transition energies is achieved only by using [Kr]/[Xe,4f] core AIMP of the neutral Ln–An elements, which have been presented in Ref. 18. Alternatively, and only for the actinides, the large [Xe,$4f$,$5d$] core AIMPs obtained in the $5f^{n-1}6d^1$ state of the An^{4+} have been found to be equally transferable and accurate for both atomic and molecular properties of the An^{4+} free and An^{4+}-doped ions, since these core potentials are capable of reproducing the tremendous radial change of the $6d$ orbital in the tetraionized An and its indirect effect on the $5d$ outer core model potential. Therefore, in this work we have produced the relativistic core AIMP of U^{4+} $(5f^16d^1)-{}^3H$ ([Xe,$4f$,$5d$] core) and have used it together with the mass-velocity and Darwin operators, and valence basis set produced on neutral U $(5f^36d^17s^2)-{}^5K$ ([Xe,$4f$,$5d$] core) in Ref. 32, with only a minor change in the d block of the basis set: Whereas the primitive Gaussian functions are those of Ref. 32, the contraction coefficients of the minimal basis set have been obtained in the U^{4+} $(5f^16d^1)-{}^3H$ calculation. Also, instead of applying the usual spin–orbit correction of the basis set to the d block,[36] we adjusted the value of the projection constant of the $5d$ core orbital until a high quality was obtained in the atomic spin–orbit coupling constant, as described in Ref. 18. The minimal valence basis set of uranium, $(14s10p11d9f)$, was augmented by three Gaussian functions of g type, $3g$, which were obtained by maximum radial overlap with the U $5f$ orbital, in order to be used as polarization functions. The contraction of the basis used was U $[6s5p5d4f1g]$. The effects of the splitting of the $3g$ polarization function were investegated and found to be of minor importance in a similar system: $Cs_2NaYCl_6:(UCl_6)^{3+}$.[19] For chlorine, we used the [Ne] core relativistic Cowan–Griffin–Wood–Boring AIMP and valence basis set ($7s6p$) of Ref. 37 augmented by $1p$ diffuse function for anions,[38] and $1d$ polarization function,[39] the final contraction being $[3s4p1d]$.

All the calculations that use the relativistic spin-free Cowan–Griffin AIMP Hamiltonian we have just described have been done using the MOLCAS-5 program system.[40] The core AIMP and valence basis set data can be found in Ref. 24.

2. Spin–orbit Hamiltonian calculations

Once the potential energy surfaces are computed for all states of interest at the MS-CASPT2(Cl48,U10) level using the spin-free CG-AIMP Hamiltonian, the dynamic electron correlation effects are transported to the spin–orbit configuration interaction (CI) calculations which are performed on a much smaller configurational space through the spin-free-state-shifted Wood–Boring (WB) AIMP Hamiltonian,[15,25] $H_{\mathrm{sfss}}^{\mathrm{WB\text{-}AIMP}}$, which results from adding to the many-electron spin–orbit WB-AIMP Hamiltonian[36] the following spin-free state shifting operator:

$$\sum_{iSM_S\Gamma\gamma} \delta(iS\Gamma)|\Phi^{\mathcal{P}}(iSM_S\Gamma\gamma)\rangle\langle\Phi^{\mathcal{P}}(iSM_S\Gamma\gamma)|, \qquad (1)$$

with

$$\delta(iS\Gamma)=[E^{\mathcal{G}}(iS\Gamma)-E^{\mathcal{G}}(1\,{}^3T_{1g})]-[E^{\mathcal{P}}(iS\Gamma)-E^{\mathcal{P}}(1\,{}^3T_{1g})]. \qquad (2)$$

TABLE I. Calculated and experimental $5f-5f$ absorption spectra of U^{4+} in gas phase. λ^U [Eq. (3)] is the atomic spin–orbit coupling scaling factor of uranium. $\delta(^3P)$ and $\delta(^1I)$ are the spin-free state shifting parameters of Eqs. (1) and (2). All numbers in cm^{-1}.

	sfss spin–orbit WB-AIMP Hamiltonian				
	$\lambda^U=1.0$	$\lambda^U=0.9$			
State[a]		$\delta(^3P)-1000$, $\delta(^1I)-1000$[d]		DC[b]	Experiment[c]
$^3H_4$	0	0	0 (88.25 ^3H)	0	0 (89.30 ^3H)
$^3F_2$	4156	4062	4056 (86.67 ^3F)	4084	4161 (86.32 ^3F)
$^3H_5$	7082	6320	6320 (99.98 ^3H)	6233	6137 (100.0 ^3H)
$^3F_3$	9687	8925	8925 (99.96 ^3F)	9025	8984 (100.0 ^3F)
$^3F_4$	10 023	9276	9276 (47.61 ^3F 43.27 ^1G)	9585	9434 (49.63 ^3F 42.28 ^1G)
$^3H_6$	13 114	11 831	11 779 (94.28 ^3H)	11 711	11 514 (94.61 ^3H)
$^1D_2$	17 794	17 044	16 727 (54.61 ^1D 34.21 ^3P)	16 554	16 455 (55.01 ^1D 33.43 ^3P)
$^1G_4$	18 121	16 581	16 581 (51.42 ^3F 45.92 ^1G)	16 929	16 656 (49.53 ^3F 47.86 ^1G)
$^3P_0$	18 424	18 159	17 232 (92.90 ^3P)	17 471	17 128 (93.51 ^3P)
$^3P_1$	21 808	21 044	20 044 (99.98 ^3P)	20 145	19 819 (100.0 ^3P)
$^1I_6$	24 309	23 278	22 330 (94.30 ^1I)	22 581	22 276 (94.61 ^1I)
$^3P_2$	27 106	25 663	24 986 (65.05 ^3P 32.74 ^1D)	24 979	24 653 (65.85 ^3P 32.04 ^1D)
$^1S_0$	44 619	43 352	43 278 (92.92 ^1S)	46 230	43 614 (93.51 ^1S)
rms[e]					
$^1S_0$ excluded	1478	681	198	231	
$^1S_0$ included	1444	657	214	787	
^3P_J, $^1I_6$ excluded		273			

[a]Labels as $^3H_4$ are customarily used to identify atomic spin–orbit levels even though they may be very inadequate in some cases (cf. $^3F_4$, $^1G_4$, and $^1D_2$, $^3P_2$). Their subindex J is the only valid quantum number.
[b]Relativistic Dirac–Coulomb coupled cluster calculation from Ref. 46.
[c]Experimental absorption spectrum from Refs. 44 and 45. Weights of the SL terms larger than 15%, which result from diagonalization of the parametric Hamiltonian of Ref. 45, are given in parentheses.
[d]Weights of SL terms larger than 15% are given in parentheses.
[e]Root-mean square deviations relative to experimental data.

In Eqs. (1) and (2) $[E^{\mathcal{G}}(iS\Gamma)-E^{\mathcal{G}}(1\,^3T_{1g})]$ are the MS-CASPT2(Cl48,U10) electronic transition energies relative to the ground state $1\,^3T_{1g}$. $\mathcal{P}$ is a small CI space defined by the complete U $5f$, $6d$ active space reference mentioned before plus their single excitations to the virtual space. $[E^{\mathcal{P}}(iS\Gamma)-E^{\mathcal{P}}(1\,^3T_{1g})]$ are the corresponding spin-free CI energy differences.[15,25] The spin–orbit part of the sfss WB-AIMP Hamiltonian has been described in detail in previous works[15,32,36] and defined as a sum of atomic one-electron spin–orbit (SO) terms,[41] $\hat{h}^I_{\mathrm{SO}}(i)$ ($I=$U, Cl, in our case)

$$\hat{h}^I_{\mathrm{SO}}(i)=\lambda^I \sum_{n\ell\in valence} V^{I,\mathrm{MP}}_{\mathrm{SO},n\ell}(r_i)\hat{O}^I_\ell \hat{\mathbf{l}}^I\hat{\mathbf{s}}\hat{O}^I_\ell . \quad (3)$$

The details of this operator can be found in Ref. 32 [cf. Eq. (8)]; the only purpose to rewrite it here is to stress on the presence of the parameter λ^I, which may act as a scaling factor for the spin–orbit contribution of atom I. This factor has been used as 1.0 in most applications, but it will be given the values $\lambda^{\mathrm{U}}=0.9$, $\lambda^{\mathrm{Cl}}=1.0$, in this work as it will be justified below in Secs. III and IV B. The valence basis sets described above were used in the spin–orbit CI calculations after removal of the polarization functions: U $[6s5p5d4f]$, Cl $[3s4p]$. The calculations corresponding to this level will be referred to as sfss spin–orbit WB-AIMP calculations, or simply as spin–orbit CI, from now on.

A modified version of the COLUMBUS package was used for all spin–orbit CI calculations.[42]

III. THE ABSORPTION SPECTRUM OF U^{4+} IN GAS PHASE

The calculation of the absorption spectrum of the U^{4+} free-ion is very useful because it helps to interpret the spectroscopy of U^{4+}-doped crystals and it helps to establish the quality of basis set, spin–orbit operator, and electron correlation at the atomic level. Consequently, we have calculated the $5f-5f$ absorption spectrum of the U^{4+} free-ion at the sfss spin–orbit WB-AIMP level. The calculated spectra, which are presented in Table I and Fig. 1 (see also Fig. 6 in the Supplementary Material Section of Ref. 43 as EPAPS document file) can be compared to available experimental data[44,45] and to very accurate relativistic Dirac–Coulomb coupled cluster calculations[46] where $4f$, $5spdf$, and $6sp$ electrons were correlated.

The results of the spin–orbit CI spectrum calculated as explained in the previous Section, by using the atomic MS-CASPT2(U10) spin-free results to define the spin-free state shifting parameters $\delta(iS\Gamma)$ [Eq. (2)] and the usual $\lambda^U=1.0$ value for the scaling factor of the spin–orbit contribution of U [Eq. (3)], are the first ones presented in Table I. Their comparison with the experimental values from Refs. 44 and 45 (Fig. 1) shows an increasing error with the transiton energy value. An analysis of the sources of these errors follows, based on the fact that the present approximated relativistic Hamiltonian shows a separated, pure spin–orbit operator, on the one hand, and that the correlation effects are handled in

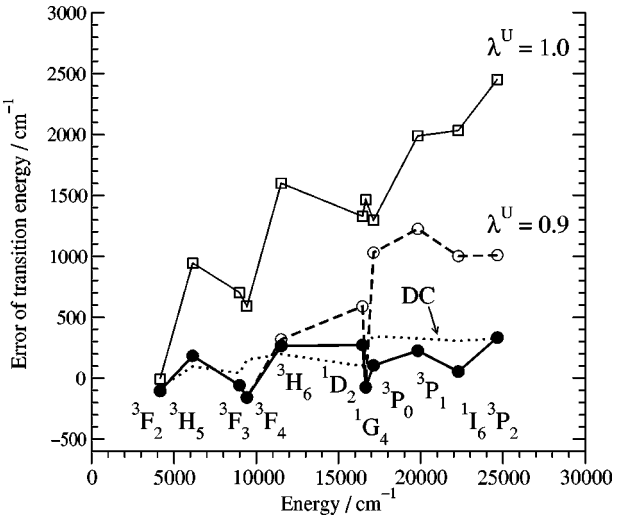

FIG. 1. Errors of calculated U^{4+} free-ion $5f^2-5f^2$ transition energies with respect to experimental values from Refs. 44 and 45. (□) sfss spin–orbit WB-AIMP calculations using the atomic spin–orbit scaling constant $\lambda^U = 1.0$ [Eq. (3)]. (○) Same as before, but $\lambda^U = 0.9$. (●) Same as before, but $-1000\ \mathrm{cm}^{-1}$ empirical correction is added to the spin-free state shifting parameters $\delta(^3P)$ and $\delta(^1I)$ [Eqs. (1) and (2)]. DC (dotted line) stands for relativistic Dirac–Coulomb coupled cluster calculations (Ref. 46).

separated calculation and transferred into the spin–orbit CI, on the other.

First of all, the spin–orbit splittings are calculated slightly larger than experimentally observed, as illustrated by the splittings of the ^3H term (see Table I and Figs. 1 and 6). In effect, $^3H_4$, $^3H_5$, and $^3H_6$ have very small contributions from other terms than ^3H and, in consequence, their splitting is almost enterily due to the direct effect of the spin–orbit component of the Hamiltonian, which suggests that the U contribution to the spin–orbit operator should be reduced. In effect, the errors of the spin–orbit splittings decrease notably when the calculations are repeated using the scaling factor in Eq. (3), $\lambda^U = 0.9$ (see Table I and Fig. 1).

After doing so, the results show errors lower than $500\ \mathrm{cm}^{-1}$, except for the transitions to the $^3P_0$, $^3P_1$, $^1I_6$, $^3P_2$ levels (see Fig. 1), which suggests that the ^3P and ^1I terms are being calculated some $1000\ \mathrm{cm}^{-1}$ too high at the MS-CASPT2(U10) level, this revealing itself as the second source of discrepancy. Consequently, we performed a last calculation where an empirical correction of $-1000\ \mathrm{cm}^{-1}$ was added to the sfss parameters $\delta(^3P)$ and $\delta(^1I)$ [Eq. (2)]. The results are very satisfactory when compared to experiment and to accurate relativistic Dirac–Coulomb coupled cluster calculations,[46] the final root-mean square deviation with respect to experiments being $214\ \mathrm{cm}^{-1}$. The comparison with the Dirac–Coulomb coupled cluster results[46] indicate that the main effect of including more electron correlation than that corresponding to U $6s,6p$, and $5f$ included here, seems to be the lowering of ^3P and ^1I by around $1000\ \mathrm{cm}^{-1}$. We produce a quite reasonable result for $^1S_0$ and we cannot identify with this analysis the source of the large error ($2600\ \mathrm{cm}^{-1}$) found in the Dirac–Coulomb coupled cluster calculation.

In summary, the atomic calculations indicate that the WB spin–orbit operator overestimates spin–orbit coupling by around 10% and this can be corrected with a scaling factor of 0.9. They also indicate that the present theoretical level of correlation overestimates the energies of the ^3P and ^1I by some $1000\ \mathrm{cm}^{-1}$ and this can be corrected with an empirical addition of $-1000\ \mathrm{cm}^{-1}$ to the sfss parameters $\delta(^3P)$ and $\delta(^1I)$.

Finally, we would like to remark that the sources of error have been identified as a result of the structure of the Hamiltonian, in the first place, and that, once identified it is again the structure of the Hamiltonian what has allowed for the correction of the errors in a very simple, though efficient, way. Also remarkable is the fact that the corrections on the Hamiltonian have been empirical in this case but, they could have been done on the basis of the accurate *ab initio* Dirac–Coulomb coupled cluster calculations instead. This is important because experimental data on atomic spectra are indeed very rarely available for the actinoids, whereas Dirac–Coulomb coupled cluster calculations are feasible and very reliable. As we show in this paper, the atomic corrections we have just studied should be transported to the study of the spectroscopy of the U^{4+} ion in the solid. This fact enhances the importance of atomic Dirac–Coulomb coupled cluster spectroscopic calculations, which, together with the sfss technique and the AIMP embedded cluster Hamiltonian, are an important source of information for practical studies of solids doped with actinide ions, in addition to providing atomic benchmarks for simpler relativistic methods.

IV. STRUCTURE AND SPECTROSCOPY OF U^{4+}-DOPED Cs_2ZrCl_6

A. Local structure of $5f^2$ and $5f^16d^1$ states of $Cs_2ZrCl_6:(UCl_6)^{2-}$

Following the two-step procedure described in Sec. II we calculated the potential energy surfaces of all $5f^2$ and $5f^16d^1$ electronic states of the embedded $(UCl_6)^{2-}$ cluster and, therefore, their U–Cl equilibrium distance, R_e, totally symmetric vibrational frequency of the $(UCl_6)^{2-}$ unit, $\overline{\nu}_{a_{1g}}$, and minimum-to-minimum energy relative to the ground state, T_e, using the spin-free and spin–orbit Hamiltonians referred to above. The procedure followed to compute the U–Cl equilibrium distances and vibrational frequencies from the numerical energy–distance values has been detailed somewhere;[23] they are stable in some 0.001 Å and $1-3\ \mathrm{cm}^{-1}$, respectively. In this subsection we concentrate on the local structure parameters and on the effects of electron correlation, crystal field, and spin–orbit coupling on their values; the electronic transition energies will be discussed later on. The structural parameters obtained here should show the same accuracy as that already proven on very similar applications on $Cs_2ZrCl_6:Pa^{4+}$ (Ref. 17) and $Cs_2NaYCl_6:U^{3+}$.[19]

A summary of the results of the geometry optimization of all $^{3,1}\Gamma_{g,u}$ electronic states of the $(UCl_6)^{2-}$ embedded cluster using the spin-free Cowan Griffin AIMP Hamiltonian is presented in Table II, where only spin-triplet electronic states have been tabulated; the parentage with U^{4+} free ion terms, although approximate, is indicated. Since all the calculations use the Cs_2ZrCl_6 AIMP embedding potential, host

TABLE II. Spectroscopic constants of the $5f^2$ and $5f^1\,6d^1$ spin-triplet manifolds of $Cs_2ZrCl_6:(UCl_6)^{2-}$ [U–Cl bond distance R_e(Å), breathing mode vibrational frequency $\overline{\nu}_{a_{1g}}$(cm^{-1}), and minimum-to-minimum energy T_e(cm^{-1})] as calculated with the spin-free Hamiltonian. Mean averages and mean square deviations are shown for R_e and $\overline{\nu}_{a_{1g}}$, and energy ranges for T_e; their respective values for individual electronic states are presented in Table V in the Supplementary Material Section of Ref. 43 as an EPAPS document file.

	CASSCF($5f$,$6d$)			MS-CASPT2(Cl48,U10)		
	R_e	$\overline{\nu}_{a_{1g}}$	T_e	R_e	$\overline{\nu}_{a_{1g}}$	T_e
$5f^2$ manifold	2.671±0.003	317±0.5		2.608±0.005	320±0.9	
from ^3H_g: $1-2\,^3T_{1g}$, $1\,^3T_{2g}$, $1\,^3E_g$			0–2007			0–3530
from ^3F_g: $3\,^3T_{1g}$, $2\,^3T_{2g}$, $1\,^3A_{2g}$			5375–6549			4815–6534
from ^3P_g: $4\,^3T_{1g}$			20 235			15 826
$5f^1 6d(t_{2g})^1$ manifold	2.641±0.004	321±1		2.571±0.005	324±0.6	
$1-3\,^3T_{1u}$, $1-2\,^3T_{2u}$, $1\,^3A_{1u}$, $1-2\,^3E_u$			33 286–41 149			29 113–36 508
$5f^1 6d(e_g)^1$ manifold	2.709±0.003	306±1		2.643±0.008	299±2	
$4-5\,^3T_{1u}$, $3-4\,^3T_{2u}$, $3\,^3E_u$			65 871–71 347			64 226–69 602

effects beyond first neighbor are included even at the lowest level of methodology, namely the CASSCF($5f$,$6d$) level, where the effects of the ligands are naturally embodied in the multiconfigurational CASSCF wave functions of $(UCl_6)^{2-}$. The effects of dynamic electron correlation included through the MS-CASPT2 method, as mentioned above, can be ascertain by comparing the MS-CASPT2(Cl48,U10) results with the CASSCF($5f$,$6d$) ones.

Three manifolds of states are found which include virtually parallel potential energy surfaces, sharing about the same U–Cl equilibrium distances and a_{1g} vibrational frequencies (spin-singlet electronic states, not included in the table, can be classified in the same three groups); each one of them can be labeled according to the following *superconfigurations*:[35,47,48] $5f^2$, $5f^1 6d(t_{2g})^1$, and $5f^1 6d(e_g)^1$. The mean values and mean square deviations of the bondlengths and vibrational frequencies over each manifold appear in Table II.

The effects of electron correlation on the spectroscopic parameters of the three manifolds are as follows: Electron correlation appears to increase the ligand field splitting of the free ion ^3H and ^3F terms, and to lower considerably the $4\,^3T_{1g}$ cluster state related to U^{4+} ^3P. The effect of electron correlation on the $5f^1 6d^1$ states is a large stabilization which, in average, amounts to 4900 cm^{-1} in the $5f^1 6d(t_{2g})^1$ manifold, and to 2300 cm^{-1} in the $5f^1 6d(e_g)^1$ manifold, approximately; this means that electron correlation also increases the overall ligand field separation between the $5f^1 6d(t_{2g})^1$ and $5f^1 6d(e_g)^1$ manifolds. The effect of electron correlation on the equilibrium distances is a general shortening of the bond lengths which, approximately, amounts to an average of 0.063 Å in the $5f^2$ manifold, and to some 0.070 and 0.065 Å in the $5f^1 6d(t_{2g})^1$ and $5f^1 6d(e_g)^1$ manifolds, respectively. The effects of electron correlation on the vibrational frequencies are very small.

The expected (octahedral) crystal field effect on d orbitals[49] is apparent in the different values of R_e of the $5f^1 6d(t_{2g})^1$ and $5f^1 6d(e_g)^1$ manifolds: The energy difference between the upper $d(e_g)$ states and the lower $d(t_{2g})$ states is known to decrease with the metal–ligand distance (with an R^{-5} dependence according to the crystal field theory[49]), so leading to a larger bond distance in the e_g states than in the t_{2g} states. In this case, their offset is 0.072 Å (Table II); an analogous offset was obtained in the $Cs_2ZrCl_6:Pa^{4+}$ system: 0.080 Å.[17] The crystal field effect on the f orbitals is much smaller: The variations of the equilibrium distances of the states belonging to the $5f^2$ manifold are of the order of 10^{-3} Å, too small so as to separate this group into subsets of off-shifted potential energy surfaces: moreover, the bondlengths become even closer as the spin–orbit coupling is introduced. Work in progress in our laboratory in U^{3+} and Np^{4+} doped ions, shows that, as the number of f electrons increases, the crystal field effects on the R_e values of different states within the $5f^n$ superconfiguration become non-negligible. Finally, the equilibrium distance of the $5f^2$ states of $Cs_2ZrCl_6:U^{4+}$ appears to be larger than that of the $5f^1 6d(t_{2g})^1$ states by 0.037 Å and smaller than the $5f^1 6d(e_g)^1$ ones by 0.035 Å; these offsets were found to be 0.021 and 0.059 Å, respectively, in $Cs_2ZrCl_6:Pa^{4+}$.[17]

The optimization of the potential energy surfaces of the Γ_g and Γ_u spin–orbit states corresponding to the second-step calculations, where the sfss spin–orbit WB-AIMP Hamiltonian is used, reveal a negligible change on the impurity-ligand distances R_e, a_{1g} vibrational frequencies, and the structure of superconfiguration manifolds (see Table III; a plot of the potential energy surfaces of all levels is presented in the Supplementary Material Section of Ref. 43). The values of the U–Cl equilibrium distance and $\overline{\nu}_{a_{1g}}$ of the $1\,A_{1g}$ ground state of $Cs_2ZrCl_6:(UCl_6)^{2-}$ obtained in our calculations are 2.602 Å and 319 cm^{-1}, respectively. The Zr–Cl distance of Cs_2ZrCl_6 perfect host is 2.446 Å, which means that a considerable outwards local distortion occurs upon U^{4+} doping approaching the value 2.75 Å of the U–Cl distance in perfect Cs_2UCl_6 crystal.[50] The $\overline{\nu}_{a_{1g}}$ value of 319 cm^{-1} we find in $Cs_2ZrCl_6:U^{4+}$ is also very close to the 315±5 cm^{-1} reported for Cs_2UCl_6 by Pollack and Satten[51] obtained from Raman spectrum in Cs_2UCl_6. Experimental

TABLE III. Results of sfss spin–orbit WB-AIMP calculations. Minimum-to-minimum energy differences T_e, in cm^{-1} and analyses of the spin–orbit wave functions of $Cs_2ZrCl_6:(UCl_6)^{2-}$. Manifold averages and root-mean square deviations of the equilibrium distances R_e, and breathing mode vibrational frequencies $\overline{\nu}_{a_{1g}}$, are also given.

State	T_e	Spin-triplet character[a]		Weight of spin-free wave functions larger than 15%[a]			
$5f^2$ manifold		$R_e=2.605\pm0.003$ Å; $\overline{\nu}_{a_{1g}}=320\pm2\ cm^{-1}$					
from $^3H_4$							
$1\ A_{1g}$	0	91.20	90.88	$1\ ^3T_{1g}$			
$1\ T_{1g}$	914	87.98	50.55	$1\ ^3T_{1g}$	28.83	$1\ ^3T_{2g}$	
$1\ E_g$	1282	87.65	43.11	$1\ ^3T_{2g}$	29.88	$2\ ^3T_{1g}$	
$1\ T_{2g}$	2428	91.04	59.61	$2\ ^3T_{1g}$	24.49	$1\ ^3E_g$	
from $^1D_2$, $^1G_4$, and $^3P_0$							
$8\ T_{2g}$	16 624	42.43	53.69	$2\ ^1T_{2g}$	22.19	$4\ ^3T_{1g}$	
$6\ E_g$	16 817	65.84	30.00	$3\ ^3T_{1g}$	23.77	$1\ ^1E_g$	20.29	$2\ ^3T_{2g}$
$4\ A_{1g}$	16 903	59.26	41.22	$3\ ^3T_{1g}$	23.82	$1\ ^1A_{1g}$	15.62	$2\ ^1A_{1g}$
$7\ T_{1g}$	16 925	66.75	42.92	$3\ ^3T_{1g}$	24.99	$1\ ^1T_{1g}$	17.73	$2\ ^3T_{2g}$
$7\ E_g$	17 790	46.98	43.83	$2\ ^1E_g$	22.45	$4\ ^3T_{1g}$	22.38	$2\ ^3T_{2g}$
$5\ A_{1g}$	18 108	87.42	79.20	$4\ ^3T_{1g}$				
$9\ T_{2g}$	18 192	54.09	41.35	$1\ ^1T_{2g}$	26.39	$1\ ^3A_{2g}$	15.22	$2\ ^3T_{2g}$
from $^3P_1$, $^1I_6$, and $^3P_2$							
$8\ T_{1g}$	20 478	71.74	67.47	$4\ ^3T_{1g}$	28.20	$2\ ^1T_{1g}$		
$6\ A_{1g}$	20 556	26.58	71.88	$2\ ^1A_{1g}$	23.80	$3\ ^3T_{1g}$		
$9\ T_{1g}$	20 937	45.26	54.04	$2\ ^1T_{1g}$	31.87	$4\ ^3T_{1g}$		
$10\ T_{2g}$	21 126	11.51	88.25	$3\ ^1T_{2g}$				
$3\ A_{2g}$	21 525	6.52	93.43	$1\ ^1A_{2g}$				
$8\ E_g$	23 849	38.41	38.92	$3\ ^1E_g$	35.65	$4\ ^3T_{1g}$	22.37	$2\ ^1E_g$
$11\ T_{2g}$	23 914	56.26	53.79	$4\ ^3T_{1g}$	26.08	$4\ ^1T_{2g}$	17.50	$2\ ^1T_{2g}$
$12\ T_{2g}$	25 551	24.61	70.37	$4\ ^1T_{2g}$	21.38	$4\ ^3T_{1g}$		
$9\ E_g$	26 316	33.55	56.94	$3\ ^1E_g$	31.36	$4\ ^3T_{1g}$		
$5f^16d(t_{2g})^1$ manifold		$R_e=2.571\pm0.004$ Å; $\overline{\nu}_{a_{1g}}=324\pm1\ cm^{-1}$					
$1\ E_u$	31 148	94.23	69.74	$1\ ^3T_{1u}$	23.65	$1\ ^3T_{2u}$		
$1\ T_{2u}$	31 345	95.75	73.84	$1\ ^3T_{1u}$				
$1\ A_{1u}$	32 294	26.50	73.44	$1\ ^1A_{1u}$	13.30	$3\ ^3T_{1u}$		
$1\ T_{1u}$	32 497	55.41	44.06	$1\ ^1T_{1u}$	17.50	$1\ ^3T_{2u}$	16.16	$1\ ^3A_{1u}$
$2\ E_u$	33 577	39.83	60.09	$1\ ^1E_u$	15.78	$2\ ^3T_{1u}$		
$2\ T_{1u}$	33 865	95.72	26.08	$1\ ^3A_{1u}$	24.46	$2\ ^3T_{1u}$	21.79	$1\ ^3T_{2u}$
$2\ T_{2u}$	33 930	91.19	44.23	$1\ ^3T_{2u}$	16.23	$1\ ^3E_u$	15.90	$1\ ^3A_{2u}$
$1\ A_{2u}$	34 918	88.34	78.05	$1\ ^3T_{2u}$				
$3\ T_{2u}$	35 309	71.94	34.87	$2\ ^3T_{1u}$	27.64	$1\ ^1T_{2u}$	22.66	$2\ ^3E_u$
$3\ T_{1u}$	35 843	93.39	60.14	$1\ ^3T_{1u}$	15.72	$1\ ^3E_u$	15.52	$1\ ^3T_{2u}$
$4\ T_{1u}$	37 465	74.16	30.67	$1\ ^3E_u$	21.79	$1\ ^1T_{1u}$	20.79	$2\ ^3T_{2u}$
$2\ A_{1u}$	37 860	99.88	49.27	$2\ ^3T_{1u}$	43.49	$3\ ^3T_{1u}$		
$3\ E_u$	38 057	94.10	52.83	$1\ ^3T_{2u}$	15.77	$1\ ^3T_{1u}$		
$4\ T_{2u}$	38 939	92.26	38.19	$1\ ^3E_u$	16.01	$1\ ^3T_{1u}$		
$5f^16d(e_g)^1$ manifold		$R_e=2.642\pm0.004$ Å; $\overline{\nu}_{a_{1g}}=299\pm3\ cm^{-1}$					
$11\ T_{2u}$	67 349	60.81	38.90	$3\ ^1T_{2u}$	36.46	$4\ ^3T_{1u}$	22.21	$3\ ^3E_u$

[a]Weights are given in % and correspond to calculations at R(U–Cl)=4.90 a.u.=2.59 Å.

values of R_e and $\overline{\nu}_{a_{1g}}$ for the ground state of $Cs_2ZrCl_6:U^{4+}$ have not been published, to our knowledge.

B. $5f-5f$ spectrum of $Cs_2ZrCl_6:(UCl_6)^{2-}$

The two sources of errors detected in the calculation of the $5f-5f$ spectrum of U^{4+} in gas phase, discussed in Sec. III, should be expected to reveal in the calculation of the spectrum of the U^{4+}-doped Cs_2ZrCl_6 material as well. Consequently, it is advisable to transport the same empirical corrections, which have been checked in the U^{4+} ion, to the solid state calculations. This means that we should use a spin–orbit scaling factor $\lambda^U=0.9$ in order to avoid the U spin–orbit Wood–Boring operator to produce 10% too large splittings, and we should add the $-1000\ cm^{-1}$ correction to the $\delta(iS\Gamma)$ parameters [Eq. (2)] corresponding to the $(UCl_6)^{2-}$ cluster levels resulting from the atomic ^3P and ^1I terms, that is, to $4\ ^3T_{1g}$ (related to $U^{4+}\ ^3P$) and to $2\ ^1A_{1g}$, $1\ ^1A_{2g}$, $3\ ^1E_g$, $2\ ^1T_{1g}$, $3\ ^1T_{2g}$, and $4\ ^1T_{2g}$ (related to $U^{4+}\ ^1I$). (This is done at all U–Cl distances at which the potential energy surfaces are calculated.)

In order to add further support to the incorporation of these empirical atomic corrections into the solid-state calculations, we have done two different spin–orbit CI calculations of the potential energy surfaces of all electronic states of $Cs_2ZrCl_6:(UCl_6)^{2-}$, namely: (a) One, using $\lambda^U=1.0$ and unchanged sfss parameters, which are set relative to the MS-CASPT2(Cl48,U10) vertical transition energies, and (b) a second calculation using $\lambda^U=0.9$, and the $-1000\ cm^{-1}$ cor-

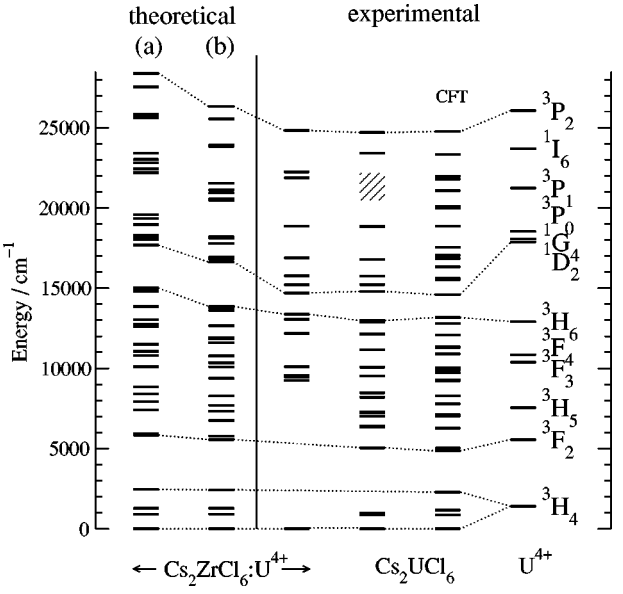

FIG. 2. Experimental and theoretical $5f^2-5f^2$ electronic transitions of U^{4+} in gas phase and in chloride crystals. (a) sfss spin–orbit WB-AIMP calculations using $\lambda^U=1.0$. (b) Same as (a) but $\lambda^U=0.9$ and the $-1000\ cm^{-1}$ empirical correction is added to the sfss parameters $\delta(iS\Gamma)$ of the $iS\Gamma$ levels related to ^3P and ^1I U^{4+} terms (see text for details). CFT stands for crystal field theory fitting. Experimental values are taken from Refs. 13, 44, 45, and 52.

rected values of the $\delta(iS\Gamma)$ listed above. We obtained the same values of the local structure parameters (R_e, $\overline{\nu}_{a_{1g}}$ of all levels) in both calculations. However, the transition energies, whose T_e values are given in Fig. 2, follow very closely the expected trend approaching the experimental values. Spin–orbit splittings and absolute values of the transition energies are both considerably improved when the $\lambda^U=0.9$ is used and ^3P- and ^1I-related spin-free states are shifted $-1000\ cm^{-1}$. The results of this latter type of spin–orbit CI calculations are, therefore, the most accurate presented here. They are the ones shown in detail in Tables III and IV, and in Fig. 2, and they will be discussed and compared with available experimental data from now on.

Table III collects a summary of the the minimum-to-minimum transition energies T_e, and the analyses of the corresponding spin–orbit CI wave functions. The weights, which result from the projection of the spin–orbit CI wave functions onto the spin-free CI wave functions used in Eq. (1), are given in %, and the sums of the contribution of all spin-triplet wave functions are also given. (For a full tabulation see Table VI in the Supplementary Material Section of Ref. 43). It should be noted that the somewhat misleading term ''spin-free wave function'' is customarily used to refer to wave functions corresponding to spin-free Hamiltonians, which, therefore, have well defined total spin. Reference is made in Tables III and IV to the relation of the crystal levels to SLJ levels of the U^{4+} free ion, even though the mixing of different J levels in the solid, as deduced from the analyses of the spin–orbit wave functions is usually high. Table VII in the Supplementary Material Section of Ref. 43 summarizes elementary symmetry decomposition of the U^{4+} free-ion SL terms or J levels in the O_h or in the $\overline{O}_h$ double group, respectively, to facilitate the reading of the wave function analyses and the discussion of the U^{4+}-doped spectroscopy in relation to its gas phase spectroscopy. In Table IV, the calculated T_e values can be compared directly with experimental zero-phonon energies measured in different crystals containing the $(UCl_6)^{2-}$ complex, which means that zero-point energy corrections to the calculated T_e values are expected to be negligible. In the experimental works, the zero-phonon lines of $Cs_2ZrCl_6:U^{4+}$,[13,14] Cs_2UCl_6,[13,14,52,53] and $[(CH_3)_4N]_2UCl_6$ (Ref. 54) [referred to as $(TMA)_2UCl_6$] have been assigned following the CFT energy calculations; we have followed those assignments to locate the experimental levels in Table IV, except for those in the last column, which have been assigned and ordered in the table following the energy calculations of this work.

Taking the experimental spectrum of U^{4+} in gas phase as a guide, (see last column in Fig. 2), we can first analyze the global effects of the solid by tracing the changes produced on three groups of levels separated by large energy gaps ($>4000\ cm^{-1}$): (i) The ground-state $^3H_4$, (ii) all levels from $^3F_2$ to $^3H_6$, and (iii) all levels from $^1D_2$ to $^3P_2$ (Fig. 2 and Table IV).

(i) The splitting of the ground level $J=4$ ($^3H_4$) in the octahedral field, although only partly observed experimentally, seems to be well described by our calculations. (ii) The $4200\ cm^{-1}$ gap to the first gas-phase level $^3F_2$ is reduced at the same time that the $^3F_2-^3H_6$ group becomes wider in energy in the $Cs_2ZrCl_6:U^{4+}$,[13,14] Cs_2UCl_6,[13,14,52] and $(TMA)_2UCl_6$,[54] measured crystals, an effect which is also observed in the calculated levels, although the latter appear to be higher in energy by less than $1000\ cm^{-1}$. (iii) The $4900\ cm^{-1}$ energy gap between $^3H_6$ and $^1D_2$ in gas phase is strongly reduced, as shown by the experimental data, to $1700-1900\ cm^{-1}$; this reduction is underestimated by our calculations: $2800\ cm^{-1}$. The whole set of crystal levels related to $^1D_2-^3P_2$ span some $9900\ cm^{-1}$ which is in closer agreement with our calculations: $9700\ cm^{-1}$. All this means that the transition energies are calculated too high by less than $2000\ cm^{-1}$ in this spectral region.

We can now take as a reference the values of the zero-phonon transitons inferred from the experimental data on Cs_2UCl_6 (Refs. 13, 14, 52) and $Cs_2ZrCl_6:U^{4+}$ (Refs. 13, 14) which appear in Table IV for a more thourough analysis. Cs_2UCl_6 is trigonal with site symmetry D_{3d} at the uranium site,[50] although the close similarity of the spectrum to those of cubic $Cs_2ZrCl_6:U^{4+}$ and $(TMA)_2UCl_6$ shows that the $(UCl_6)^{2-}$ unit is only slightly distorted from O_h symmetry. The difficulties to locate the electronic origins corresponding to the $5f^2$ levels in crystals containing $(UCl_6)^{2-}$ and $(UBr_6)^{2-}$ complexes have been pointed out by Satten *et al.*[13] and have been associated with the very large and comparable magnitude of crystal field and spin–orbit interactions, which makes it necessary to consider both effects simultaneously. In addition to this, practically the entire spectrum is vibronic and only a few pure electronic magnetic dipole transitions can be observed weakly. This means that the zero-phonon levels tabulated have been inferred from low temperature absorption spectrum by making use of vibronic selection rules and temperature shifts,[13] and electronic level splittings

TABLE IV. Theoretical and experimental $5f-5f$ spectra of $(UCl_6)^{2-}$ in different chloride crystals. All number in cm^{-1}.

State	$(TMA)_2UCl_6$	Cs_2UCl_6		$Cs_2ZrCl_6:U^{4+}$			
	Ref. 54	Refs. 13, 52, 53[a]	Ref. 14[b]	Ref. 13[c]	Ref. 14[b]	this work[d]	reassignments[e]
from $^3H_4$							
1 A_{1g}	0	0	0	0	0	0	0
1 T_{1g}		897,979				914	
1 E_g						1282	
1 T_{2g}						2428	
from $^3F_2$, $^3H_5$							
2 E_g	5056	5060	5064		5058	5562	5058 (504)
2 T_{2g}	4901	4899			4929	5775	not observed
2 T_{1g}	6371	6347,6399	6333,6387		6383	6740	6383 (357)
3 T_{2g}	7077	7011[f]			7109	7337	7109 (228)
3 T_{1g}		7209,7297			7143	7701	7143 (558)
3 E_g	8189	[8197]				8280	
							rms 432
from $^3F_3$, $^3F_4$, and $^3H_6$							
2 A_{1g}	8485	8469				9372	
4 T_{1g}	9409			9467	9468	10 101	9242 (859)
4 T_{2g}	9237			9242	9242	10 345	9468 (877)
1 A_{2g}	9612	9540		9571	9572	10 367	9572 (795)
4 E_g					10 468	10 762	10 107 (655)
5 T_{1g}	10 069	[10 065]	10 054	10 106	10 107	10 782	*10 148* (*634*)
5 E_g	11 200	[11 176]	11 180		11 220	11 607	
5 T_{2g}					11 263	11 836	11 220 (616)
6 T_{2g}						11 926	11 263 (663)
2 A_{2g}	12 129	12 128	12 133	12 178	12 180	12 657	12 180 (477)
3 A_{1g}						13 601	
6 T_{1g}		[12 984]	13 761	13 370		13 768	*13 050* (*718*)
7 T_{2g}	12 969	[12 878]	12 889,12 995	13 059	13 061	13 856	13 059 (797)
							rms 719
from $^1D_2$, $^1G_4$, and $^3P_0$[g]							
8 T_{2g}	15 776		(15 760)	15 774	15 775	16 624	15 228 (1396)
6 E_g	15 234	15 213	15 218	15 227	15 228	16 817	15 775 (1042)[g]
4 A_{1g}	14 839	14 789	14 789	14 703	14 704	16 903	14 704 (2199)[g]
7 T_{1g}		15 754	(15 677)		15 799	16 925	15 799 (1126)
7 E_g						17 790	
5 A_{1g}	16 835	16 797	16 809	16 883	16 884	18 108	16 884 (1224)
9 T_{2g}			17 338		(17 381)	18 192	
							rms 1459[g]
from $^3P_1$, $^1I_6$, and $^3P_2$							
8 T_{1g}	18 870[h]	18 826,18 832	18 839	18 867	18 871	20 478	18 871 (1607)
6 A_{1g}						20 556	
9 T_{1g}			20 500		(20 552)	20 937	
10 T_{2g}			(20 764)		(20 794)	21 126	
3 A_{2g}						21 525	
8 E_g	22 229	[22 183]	22 216	22 246	22 257	23 849	21 883 (1966)
11 T_{2g}	21 899	[21 814]	21 834	21 876	21 883	23 914	22 257 (1657)
12 T_{2g}	23 447	23 399	23 416			25 551	
9 E_g	24 739	24 700	24 745	24 820	24 820	26 316	24 820 (1496)
							rms 1691
from $^1S_0$							
7 A_{1g}		41 403[i]	41 893[i]			39 942	

[a]Uranium site symmetry is D_{3d}, which results in splitting of the magnetic dipole transitions $A_{1g}\rightarrow T_{1g}$; corresponding polarization data from Ref. 52 are tabulated wherever available. Values in square brackets cannot be assigned on the basis of experiment alone (Ref. 13). See text for details.

[b]Electronic origins 5058 to 7143 cm^{-1} in $Cs_2ZrCl_6:U^{4+}$ correspond to 85 K luminescence spectrum under argon ion laser excitation [from the 8 $T_{1g}(^3P_1$ level]. Values in parentheses correspond to uncertain measurements or assignments (Ref. 14).

[c]Electronic origins measured at 4 K.

[d]Results of spin–orbit CI calculations of minimum-to-minimum energy differencies T_e relative to the 1 A_{1g} ground state.

[e]Experimental origins from Ref. 14 are listed and reassigned according to the results of spin–orbit CI calculations of this work. The differences between the spin–orbit CI results and the experimental values are given in parentheses. rms stands for root mean square deviation within a group of states. Electronic origins deduced in this work by substracting the calculated $\overline{\nu}_{a_{1g}}=320\ cm^{-1}$ are given in italics.

[f]From Ref. 52.

[g]The assignments in this group of states, based on the present calculations, could change if $(6\ E_g+4\ A_{1g})\otimes e$ pseudo-Jahn–Teller coupling were considered. See text for details.

[h]Splitting of this level (18 852 and 18 864 cm^{-1}) has been observed in Ref. 52 and attributed to Jahn–Teller effect.

[i]From crystal field theory energy calculation in the corresponding experimental reference.

observed in polarization spectra.[52] As a result of this procedure, and given that the symmetry of the $(UCl_6)^{2-}$ ground state is A_{1g}, only the electronic origins belonging to the A_{1g}, A_{2g}, and T_{1g} irreducible representations of the $\overline{O}_h$ double group can be identified with certainty in Cs_2UCl_6, whereas those belonging to E_g or T_{2g} symmetries cannot; in the cubic lattices, like $Cs_2ZrCl_6:U^{4+}$ and $(TMA)_2UCl_6$, only the electronic levels of A_{1g} and A_{2g} symmetries can be identified by vibronic selection rules, whereas those belonging to E_g, T_{1g}, or T_{2g} irreducible representations cannot. These facts limit the assignments of all observed lines if energy level calculations are not available. This inconvenient is usually overcome by resorting to iterative CFT fitting procedures,[13] which are considered to perform satisfactorily. It must be noted though, that these procedures can lead to different reasonable assignments of the levels whose symmetry is not certain from experiment when different values of the CFT parameters are used, as we comment below.[13,53] As a matter of fact, Satten *et al.*[13] clearly distinguish the electronic origins which appear in square brackets in Table IV as levels which ''cannot be assigned on the basis of experiment alone,'' or whose assignment ''depends heavily'' on the CFT energy level calculation, from the rest of electronic origins whose identification is considered to be highly certain. Consequently, we will use the latter to establish the accuracy of our calculations by comparison, and will, eventually, propose different assignments from CFT for the former.

The only crystal field level of $^3H_4$ experimentally observed, $1\,T_{1g}$, is calculated fairly close to experiment.

The group of states from $2\,E_g$ to $3\,E_g$ spans 2718 cm^{-1} and appears to be split into two subgroups: $2\,E_g-2\,T_{2g}$ and $2\,T_{1g}-3\,E_g$ with an energy gap of 965 cm^{-1}, in fairly close agreement with experimental observations. First, let us compare our results with the experimental lines observed in Cs_2UCl_6 by Satten *et al.*[13,53] whose assignment has been confirmed by polarization data.[52] These lines are the $2\,T_{1g}$, $3\,T_{2g}$, and $3\,T_{1g}$ levels and the discrepancies our results show with them are very consistent: 397, 326, and 434 cm^{-1}, respectively. The situation in the first subgroup, $2\,E_g-2\,T_{2g}$, where the symmetry assignment of the observed lines cannot be deduced from experiment, is somewhat puzzling, as we explain next. In effect, Satten *et al.* reported the line at 5060 cm^{-1} in Ref. 13, where it was assigned as the E_g component of $^3F_2$ (note that this line was also observed in Cs_2UCl_6 by Flint and Tanner[14]); the authors stressed that no other lines were observed below 5000 cm^{-1} for at least 1000 cm^{-1}, in spite of the fact that the T_{2g} component of $^3F_2$ was expected to be lower in energy, in analogy the the observations in Cs_2UBr_6, where two origins separated by some 225 cm^{-1} were detected in the order $2\,T_{2g}<2\,E_g$.[53] Several CFT energy calculations were reported[13] where the $2\,E_g$ line at 5060 cm^{-1} was used as input, and they all led to the expected order $2\,T_{2g}<2\,E_g$ with different energy separations, depending on the fitting stage: 105, 250, 165 cm^{-1}.[13] In a subsequent paper,[53] a line below 5000 cm^{-1}, at 4899 cm^{-1}, assigned to $2\,T_{2g}$, appeared tabulated as one of the observed lines without further comments (note that this line was not observed in the absorption spectrum of Cs_2UCl_6 of Flint and Tanner[14]). Both 4899 ($2\,T_{2g}$) and 5060 cm^{-1} ($2\,E_g$) data were used as input of a new CFT energy calculation,[53] which led, this time, to inverted order: The output CFT energies were reported to be 4865 ($2\,E_g$) and 4973 ($2\,T_{2g}$), 108 cm^{-1} apart. Given that the CFT input and output assignments are not consistent, it is unclear what the final assignment of these levels should be in the context of the usual combination of experimental and CFT information, as it is unclear that there should be any *a priori* reason to expect any order at all [note that the data in the bromide crystal are also very confusing: whereas the experimental levels are reported to be at 4717 ($2\,T_{2g}$) and 4940 ($2\,E_g$), 223 cm^{-1} apart, the CFT calculated levels came out in reversed order and almost degenerate: 4733 cm^{-1} ($2\,E_g$), 4763 ($2\,T_{2g}$)[53]]; finally, and very important for energy levels lying above the ones we are discussing, it is unclear what the outcome of CFT energy calculations would be for these and other E_g and T_{2g} levels if the input assignment given to the CFT calculations would be reversed in an attempt to make CFT input and output data consistent. Consequently with all this, we can now compare our energy calculations with experiments disregarding any *a priori* assignments for the levels at 4899 and 5060 cm^{-1}. The discrepancy of our calculation with the 5060 cm^{-1} line comes out to be 506 cm^{-1} if it is assigned to $2\,E_g$; this error is very similar to the discrepancies observed in close lying and securely assigned levels we have discussed in the first place, above. The line at 4899 cm^{-1} gives a discrepancy of 876 cm^{-1} with our calculated $2\,T_{2g}$, this error being much higher than expected in this spectral region. The discrepancies of our calculations with these lines is also high if they are calculated in inverted order (663 and 715 cm^{-1}). Consequently, our results coincide best with and support the former observations of Satten *et al.*[13] which concluded that only one electronic origin could be inferred in this energy region: That at 5060 cm^{-1}, this being ascribable to the $2\,E_g$ state. Our results do not support the existence of a second origin below and so close in energy as the line at 4899 cm^{-1} introduced in subsequent work, whose observation is not reported by Flint and Tanner.[14] Rather, our results point out that the $2\,T_{2g}$ origin is, in fact, some 200 cm^{-1} away, but above $2\,E_g$, this being the reason why no other lines were observed below 5000 cm^{-1} in the works of Refs. 13 and 14 in Cs_2UCl_6. In the second subgroup, the discrepancy of our result with the line at 8197 cm^{-1} in Cs_2UCl_6 is 83 cm^{-1}, much smaller than expected, which, together with the fact that it is not observed in $Cs_2ZrCl_6:U^{4+}$, makes its assignment as the zero-phonon line corresponding to $3\,E_g$ uncertain.

The energies of the levels of this group observed in $Cs_2ZrCl_6:U^{4+}$ have not been inferred from low temperature absorption spectra, but from 85 K luminescence spectrum under argon ion laser excitation[14] [from $8\,T_{1g}(^3P_1)$]; more recently, this spectrum has been referred to as tentative by Tanner *et al.*[12] These lines are very close to the levels of Cs_2UCl_6 we have just discussed and compared with, except for the near degeneracy observed between $3\,T_{2g}$ and $3\,T_{1g}$, which is not observed in the certainly assigned levels in Cs_2UCl_6 nor in our results, this indicating that it might not

correspond to a zero-phonon line. All we have discussed above applies to the rest of lines of $Cs_2ZrCl_6:U^{4+}$, which means that the one at 4929 cm^{-1} should be associated with a vibronic feature of the emission spectrum rather than to the $2\,T_{2g}$ electronic origin.

The group of states from $2\,A_{1g}$ to $7\,T_{2g}$ appears to be split in subgroups separated by four gaps of some 700–900 cm^{-1} that are consistent with the available experimental information; the subgroups are: $2\,A_{1g}$, $4\,T_{1g}-5\,T_{1g}$, $5\,E_g-6\,T_{2g}$, $2\,A_{2g}$, and $3\,A_{1g}-7\,T_{2g}$. The discrepancies with the certainly assigned experimental levels measured in Cs_2UCl_6 at 8469 ($2\,A_{1g}$), 9540 ($1\,A_{2g}$), and 12 128 cm^{-1} ($2\,A_{2g}$), are 903, 827, and 529 cm^{-1}. Only the last two have been observed in the diluted crystal $Cs_2ZrCl_6:U^{4+}$ and the discrepancies with our calculations appear to be very similar: 795 ($1\,A_{2g}$) and 477 ($2\,A_{2g}$). We discuss now the electronic origins whose assignment is not certain, but derived from CFT calculations. After the first gap, all the levels ($4\,T_{1g}-5\,T_{1g}$) have similar energies in all crystals which appear in Table IV except the line at 10 468 cm^{-1}, which has only been reported in $Cs_2ZrCl_6:U^{4+}$ in Ref. 14. Our results suggest that this level could correspond to the first member of the a_{1g} progression ($\overline{\nu}_{a_{1g}}=320\ cm^{-1}$) on the $5\,T_{1g}$ electronic origin, whose non-negligible intensity comes from the fact that the potential energy surfaces of $5\,T_{1g}$ [$R_e(5\,T_{1g})=2.608$ Å] and $1\,A_{1g}$ [$R_e(1\,A_{1g})=2.602$ Å] are offshifted by some 0.006 Å along the $Q_{a_{1g}}$ normal coordinate (see below); if this is so, the electronic origin would be at 10 148 cm^{-1}, almost degenerate with the line at 10 107 cm^{-1}, in agreement with the *ab initio* calculations which indicate that $4\,E_g$ and $5\,T_{1g}$ are almost degenerate, and consistent with the fact that only one origin has been reported close to 10 100 cm^{-1} in all other crystals and works collected in the table. The discrepancy with theory would be then larger, but more consistent with that observed in all states in the $4\,T_{1g}-5\,T_{1g}$ subgroup where our energy calculations also suggest that the CFT assignments should be changed (see last column of Table IV). As we move to the next subgroup $5\,E_g-6\,T_{2g}$, our results show the $5\,T_{2g}$ and $6\,T_{2g}$ states are almost degenerate, which corresponds well with the two close lying lines observed by Flint and Tanner in $Cs_2ZrCl_6:U^{4+}$ at 11 220 and 11 263 cm^{-1}; this suggests a different assignment with respect to that of CFT, as it can be seen in the last column of Table IV. Finally, our calculations indicate that the three states in the last subgroup, $3\,A_{1g}-7\,T_{2g}$, have offshifted potential energy surfaces relative to the $1\,A_{1g}$ ground state by 0.008, 0.009, 0.009 Å, respectively, which makes it more likely to observe the first and second members of the a_{1g} progression (see below). As a matter of fact, Flint and Tanner[14] have ruled out as a zero-phonon line the level observed by Satten *et al.* at 13 370 cm^{-1} in $Cs_2ZrCl_6:U^{4+}$; instead, they have interpreted this line as corresponding to the first member of the a_{1g} progression of the 13 059 cm^{-1} origin (using $\overline{\nu}_{a_{1g}}=310\ cm^{-1}$). However, the $\overline{\nu}_{a_{1g}}$ is calculated to be slightly higher, 320 cm^{-1}, in this work (Sec. IV A), which means that the electronic origin that can be deduced from the line at 13 370 is 13 050 cm^{-1}, and is, therefore, almost degenerate with that at 13 059 cm^{-1}. Our *ab initio* calculations agree with this, as the $6\,T_{1g}$ and $7\,T_{2g}$ are found to be almost degenerate; consequently we have made the assignments 13 050 ($6\,T_{1g}$), 13 059 ($7\,T_{2g}$) that are shown in the last column of Table IV. Also, Flint and Tanner[14] have reported high frequency wave numbers in the vibronic structure of the $7\,T_{2g}$ line at 13 061 cm^{-1} which, following Pollack and Satten,[51] can be interpreted as superposition lines resulting from the combination of a strong odd mode with the fundamental a_{1g} mode (this accounting for 60%–80% of the high frequency lines[51]) or as the combination of two even and one odd, or three odd frequencies.[51] In this way, the high-frequency wave numbers 426 or 586 cm^{-1} listed by Flint and Tanner for the 13 061 cm^{-1} line, match the combinations: 106+320 and 266+320 cm^{-1}, where the values 106 and 266 cm^{-1} fall into the 105–109 and 265–270 cm^{-1} values of low-frequency modes which appear in the vibronic structure of many lines of $Cs_2ZrCl_6:U^{4+}$.[14] We can also consider the second member of the a_{1g} progression of both origins 13 050 ($6\,T_{1g}$) and 13 059 ($7\,T_{2g}$): They would have a considerably lower intensity (see below) and would lie at about 13 690 and 13 699 cm^{-1}, respectively. This result could be taken into account to understand the line at 13 761 cm^{-1} observed in Cs_2UCl_6 by Flint and Tanner,[14] at liquid Helium temperature, which has been reported to be too weak to be observed in the diluted material; this line could be associated with the weak second member of the a_{1g} progression on a false origin associated with $6\,T_{1g}$ or $7\,T_{2g}$ states. The intensity profile of the 0–0, 0–1, 0–2 members of the a_{1g} progression ($\overline{\nu}_{a_{1g}}=320\ cm^{-1}$) on the $7\,T_{2g}$ electronic origin can be observed in Fig. 8 in the Supplementary Material Section of Ref. 43. The same effects are observed for other electronic origins mentioned above whose equilibrium distance is offshifted by 0.006–0.009 Å relative to the $1\,A_{1g}$ ground state.

A notable characteristic of the next group of states, including $8\,T_{2g}$ to $9\,T_{2g}$, which will be instrumental in the upconversion mechanism discussed below, is a considerably lower spin-triplet character, as it can be seen in Table III. This group is calculated to be 2768 cm^{-1} higher in energy than the previous one, in clear contrast with the much smaller 1645 cm^{-1} separation observed experimentally in $Cs_2ZrCl_6:U^{4+}$. It appears to be split into two sub-groups of four ($8\,T_{2g}-7\,T_{1g}$) and three ($7\,E_g-9\,T_{2g}$) lines separated by an energy gap of some 865 cm^{-1}, which is consistent with experiments, but the energy extension of the first subgroup is calculated to be too small (300 cm^{-1}) compared with the observations (some 1100 cm^{-1}). As before, we start by comparing the results of our calculations with the levels whose assignment can be deduced from experiments, which in this case are of A_{1g} symmetry. The lines assigned as the $4\,A_{1g}$ origin have been observed at 14 789 in Cs_2UCl_6 and 14 704 in $Cs_2ZrCl_6:U^{4+}$. Their assignment to A_{1g} symmetry is associated with the absence of its t_{2u} vibronic transition.[13] A puzzling fact remains, however: Flint and Tanner[14] derived a vibrational frequency of 94 cm^{-1} from the vibronic structure of the 14 704 cm^{-1} origin, which coincides with the 93 cm^{-1} t_{2u} vibrational frequency deduced from the whole spectrum[14] (we will comment further on this below). Our

calculation shows a very large discrepancy with the observed origins, as the $4\,A_{1g}$ is found to be 2199 cm^{-1} higher in energy. This discrepancy is much higher than that obtained for the $5\,A_{1g}$ (1224 cm^{-1}) in whose vibronic structure the t_{2u} mode is absent in all reports.[13,14] The $4\,A_{1g}$ origin has been associated with the gas phase $^3P_0$ state by Satten *et al.*;[13] however, the analysis of the corresponding spin–orbit wave functions (Table III) points out $5\,A_{1g}$ as the level mainly related to $^3P_0$. This connects with the fact that the U^{4+} free ion energies that were calculated in Ref. 52 from the CFT fitting in Cs_2UCl_6 by assuming zero crystal field (cf. Fig. 1 of Ref. 52), led to "effective" U^{4+} levels ordered as $^3P_0 < {}^1D_2 < {}^1G_4$. This order does not agree with the experimental U^{4+} gas phase spectrum,[44,45] which is $^1D_2 < {}^1G_4 < {}^3P_0$. However, the effective U^{4+} levels that are inferred from our calculations do agree: The analysis of the spin–orbit wave functions of Table III points out that the states with lowest spin-triplet character in this group, $8\,T_{2g}$ and $7\,E_g$, can basically be related to U^{4+} $^1D_2$, the intermediate spin states (54%–66% triplet character), can be associated with U^{4+} $^1G_4$ level (getting the larger spin character from the notable mixture of ^3F and ^1G free ion terms observed in Sec. III), the highest spin $5\,A_{1g}$ should be associated with $^3P_0$, and their corresponding weighted averages show the gas phase order: 17 090 ($^1D_2$) < 17 321 ($^1G_4$) < 18 108 ($^3P_0$). We can now discuss the rest of levels assigned to other than A_{1g} symmetry. The CFT assignments seem to be particularly unstable in this part of the spectrum. In fact, in a first attempt Satten *et al.*[13] assigned the lines at 15 213 and 15 754 cm^{-1} in Cs_2UCl_6 to the T_{1g}/T_{2g} and E_g symmetries since these lines appear to be split into three and two, respectively, in triphenyl phosphine uranium hexabromide crystals;[13] the final assignement was done on the basis of the CFT energy calculation: 15 213 ($7\,T_{1g}$), 15 754 cm^{-1} ($6\,E_g$); the D_{3d} splitting of the 15 213 cm^{-1} line was not reported in the polarization spectra of Ref. 52, therefore, T_{1g} symmetry could not be confirmed. In a subsequent paper,[53] a new CFT calculation using a different set of parameters changed their assignment to 15 213 ($6\,E_g$) and 15 754 cm^{-1} ($7\,T_{1g}$), as shown in Table IV.[53] On the other hand, a mismatch between the input and output CFT assignments, similar to that described above for $2\,E_g$ and $2\,T_{2g}$, also occurs here for the $7\,T_{1g}$ and $8\,T_{2g}$ levels. Flint and Tanner[14] have assigned them in $Cs_2ZrCl_6:U^{4+}$ to the following almost degenerate lines: 15 775 ($8\,T_{2g}$) < 15 799 ($7\,T_{1g}$), both of which have been used as input to two different CFT energy calculations. However, these two CFT energy calculations (which use different parameter values) invert their energy order as follows: 15 721 ($7\,T_{1g}$) < 15 866 cm^{-1} ($8\,T_{2g}$), and 15 675 ($7\,T_{1g}$) < 15 813 cm^{-1} ($8\,T_{2g}$), at the same time that their relative energy separation becomes larger: 145, and 138 cm^{-1}; these CFT values are very different in Cs_2UCl_6 crystal:[53] 15 620 cm^{-1} ($7\,T_{1g}$) < 16 224 cm^{-1} ($8\,T_{2g}$), which means a 604 cm^{-1} energy separation. Consequently, we have reassigned all the levels $8\,T_{2g}$–$9\,T_{2g}$ that do not belong to the A_{1g} symmetry according to our *ab initio* calculations (see last column of Table IV); it is very clear that the discrepancies in this group are larger than those in the lower energy group, which is reasonable as we get to higher energies, and amount to 1000–1400 cm^{-1}, but it is also clear that the $4\,A_{1g}$ level appears to be a special case with an error which is almost double. From the theoretical point of view, there is no obvious reason why this $4\,A_{1g}$ level should be more difficult to reproduce than any other one around it. However, we would like to point out a circumstance which basically affects the $6\,E_g$ state and which is specific of this part of the spectrum. In effect, our results show that the potential energy surfaces of $6\,E_g$ and $4\,A_{1g}$ are parallel and almost degenerate (their energy separation is 86 cm^{-1}) along the $Q_{a_{1g}}$ totally symmetric octahedral normal coordinate; what they do not show is how these potential-energy surfaces would be like along the Jahn–Teller active tetragonal Q_{e_g} normal coordinates, since we have not explored the corresponding tetragonal distortions. If the wave functions and energies were calculated along the $Q_{e_g,\theta}$ axis ($Q_{e_g,\epsilon}=0$), to explore the $E\otimes e$ Jahn–Teller coupling, as we have done in transition metal impurities in previous works,[15] the octahedral $6\,E_g$ state would split into its $A_{1g}(6\,E_g)$ and $B_{1g}(6\,E_g)$ D_{4h} components, so that the $A_{1g}(6\,E_g)$ and $4\,A_{1g}$ wave functions would have no symmetry restrictions to interact, and, given their near degeneracy in the undistorted octrahedral structure, their actual pseudo-Jahn–Teller interaction would be strongly enhanced. This should result in a larger Jahn–Teller stabilization energy of the $A_{1g}(6\,E_g)$ wave function from that expected from an otherwise isolated octahedral E_g state; whereas the effect on the octahedral $4\,A_{1g}$ state would simply be that of a different curvature from an otherwise isolated A_{1g} octahedral state. As a result, a considerable lowering in energy of the $A_{1g}(6\,E_g)$ electronic origin should be expected relative to the $6\,E_g$ one, and this origin would correspond to that at 14 704 cm^{-1} assigned to A_{1g} symmetry. Furthermore, if the 14 704 cm^{-1} is assigned to the $A_{1g}(6\,E_g)$ electronic origin, the appearance of the 94 cm^{-1} wave number in its vibronic structure (mentioned above) could be understood as a D_{4h} component of the octahedral t_{2u} vibrational frequency. This would also explain the reduction in the $(UCl_6)^{2-}$ symmetry suggested by Flint and Tanner[14] to try to understand the complex vibronic structure around the 14 704 cm^{-1} origin. This pseudo-Jahn–Teller interaction between E_g and A_{1g} states could also occur between $7\,E_g$ and $5\,A_{1g}$, also in this group. However, since their energy separation is 3.7 times larger, the lowering of the $A_{1g}(7\,E_g)$ origin should be proportionally smaller. All other E_g and A_{1g} states in the $5f^2$ spectrum are further apart, which makes the $(6\,E_g+4\,A_{1g})\otimes e$ pseudo-Jahn–Teller interaction special. We have considered the study of the $(6\,E_g+4\,A_{1g})\otimes e$ pseudo-Jahn–Teller coupling out of the scope of this work, yet, we think it is very likely that this is the reason for the inconsistently large discrepancy between our results and the experiments in this part of the spectrum and we should deal with this problem in a forthcoming study.

As we move to the $8\,T_{1g}$–$9\,E_g$ group, the total spin-triplet character decreases even further. This results in more levels lacking in the experimental spectra, which makes it more difficult the comparison with our results. As a matter of fact, only one line has been assigned in this group with certainty: The $8\,T_{1g}$ level, whose splitting in Cs_2UCl_6 has been

observed in the polarization spectrum of Ref. 52, and which has been associated with the $^3P_1$ free ion level.[13] Our results agree in that this spin–orbit level can be associated with $^3P_1$ and the error of its calculated energy comes to be 1650 cm^{-1}. Above the $8\,T_{1g}$ state and within the first subgroup of levels, $8\,T_{1g}-3\,A_{2g}$, the measurement/assignment of the few electronic origins reported is uncertain, according to Flint and Tanner[14] (see Table IV). Their discrepancies with our calculations are not consistent with those observed for the rest of levels in this group: They are much smaller ($\sim$300 cm^{-1}); therefore, we have not included them in our final assignments. Two lines at 23 399 and 24 700 cm^{-1}, assigned to $12\,T_{2g}$ and $9\,E_g$, respectively, on the basis of the CFT energy calculation, have been associated with the two crystal components of $^3P_2$, since they are the two levels observed at highest energy before the continuous absorption sets in at about 28 800 cm^{-1} in Cs_2UCl_6. The analysis of the wave functions of Table III do not support their association with $^3P_2$: In effect, our results show that $11\,T_{2g}$, rather than $12\,T_{2g}$, can be clearly identified as the T_{2g} component of $^3P_2$ U^{4+} level, and that the mixture of $^1I_6$ and $^3P_2$ is too large so as to allow for a clear identification of the E_g component of $^3P_2$ in the crystal, although the $8\,E_g$ level is found to have larger $^3P_2$ character than the $9\,E_g$ one according to our wave function analysis. This means that our results place the levels related with $^3P_2$, $8\,E_g$ and $11\,T_{2g}$, much lower in energy than described by Satten *et al.*[13] and by Tanner *et al.*,[12] who place them above 23 000 cm^{-1} (associated with $12\,T_{2g}$ and $9\,E_g$), and in agreement with Xu *et al.*[6] who have indicated that the blue 21 837 cm^{-1} argon ion laser excites the $Cs_2ZrCl_6:U^{4+}$ samples directly into the $^3P_2$ crystal level,[6] in this case, into a vibronic sideband of the $8\,E_g$ origin at 21 883 cm^{-1}.

It is possible to summarize the quality of the calculated $5f-5f$ spectrum of $Cs_2ZrCl_6:U^{4+}$ by assigning two quantities to each of the five groups of states we have just discussed: The calculated/experimental energy spread of the group (including the lowest and highest observed levels) and the root-mean square deviations of the calculated levels *versus* the experimental levels. These quantities are as follows. $1\,A_{1g}-1\,T_{2g}$ group: 914/938 and 24 cm^{-1} (in Cs_2UCl_6); $2\,E_g-3\,E_g$ group: 2193/2085 and 432 cm^{-1}; $2\,A_{1g}-7\,T_{2g}$ group: 3755/3817 and 719 cm^{-1}; $8\,T_{2g}-9\,T_{2g}$ group: 1484/(2180/1656) (including/not the 14 704 cm^{-1} level) and 1459 cm^{-1}; $8\,T_{1g}-9\,E_g$ group: 5838/5959 and 1691 cm^{-1}. The agreement in the energy spreads is in general very good and the root-mean square deviations show increasing discrepancies with increasing energy, a fact which should be related with increasing residual electron correlation effects; however, deficiencies in the spin–orbit coupling appear to be less likely. Yet, the general agreement with experiment can be considered very satisfactory and the remaining discrepancies sufficiently understood so as to allow for the discussion of the possible upconversion mechanisms in the $Cs_2ZrCl_6:U^{4+}$ material we present in this work.

C. $5f^2-5f^16d^1$ spectrum of $Cs_2ZrCl_6:(UCl_6)^{2-}$

The calculated $5f^2-5f^16d^1$ spectrum of U^{4+}-doped Cs_2ZrCl_6 is summarized in Table III where only the levels of the $5f^16d(t_{2g})^1$ manifold lying below 39 000 cm^{-1} and the lowest level of the $5f^16d(e_g)^1$ manifold are presented. (See Table VI in the Supplementary Material Section of Ref. 43 for a full tabulation of both manifolds.) There are not experimental data available on the $5f^2-5f^16d^1$ manifold, as far as we know. The energies of the lowest $5f^16d(t_{2g})^1$ and $5f^16d(e_g)^1$ states appear at 31 100 and 67 300 cm^{-1}, respectively. Their energy separation, which can be seen as a ligand field effect, is 36 200 cm^{-1}. Although according to Xu *et al.*[6] the optical window of the Cs_2ZrCl_6 crystal is 4000–30 000 cm^{-1}, the ultraviolet absorption spectrum of the $Cs_2ZrCl_6:Pa^{4+}$ crystal taken at 4.2 K[20] shows the sharp cutoff of the Cs_2ZrCl_6 host crystal at about 37 000 cm^{-1}. Therefore, the onset of the $(UCl_6)^{2-}$ $5f^2\rightarrow5f^16d(t_{2g})^1$ band associated with vibronic absorption transitions from the $1\,A_{1g}$ ground state to even vibrational modes of the lowest $1\,E_u$, $1\,T_{2u}$ excited states should be observable. The only symmetry allowed zero-phonon transitions from the ground state ($1\,A_{1g}$) calculated to be below 37 000 cm^{-1} would appear at about 32 500 ($1\,T_{1u}$), 33 900 ($2\,T_{1u}$), and 35 800 ($3\,T_{1u}$), although that to $1\,T_{1u}$ should show a considerable spin-forbidden character. The results of the calculation of the band profile of the first electric dipole allowed absorption, $1\,A_{1g}\rightarrow1\,T_{1u}$, and emission, $1\,E_u\rightarrow1\,T_{1g}$, can be seen in Fig. 3. The band profiles have been calculated by applying the time-dependent approach of Heller,[55,56] which has been summarized in Ref. 17. For that purpose, we have used the calculated equilibrium distances: 2.602 ($1\,A_{1g}$), 2.605 ($1\,T_{1g}$), 2.567 ($1\,E_u$), 2.567 Å ($1\,T_{1u}$), a common a_{1g} vibrational frequency value of 320 cm^{-1}, and the corresponding minimum-to-minimum energy differences presented in Table III: $1\,A_{1g}\rightarrow1\,T_{1u}$: 32 497 and $1\,E_u\rightarrow1\,T_{1g}$: 30 234 cm^{-1}. As it can be seen, our calculations predict a very large gap between the symmetry allowed absorption and emission maxima, as a consequence of the emission (1) being produced from $1\,E_u$ after nonradiative decay from $1\,T_{1u}$, and (2) having as the final state $1\,T_{1g}$, which is higher than

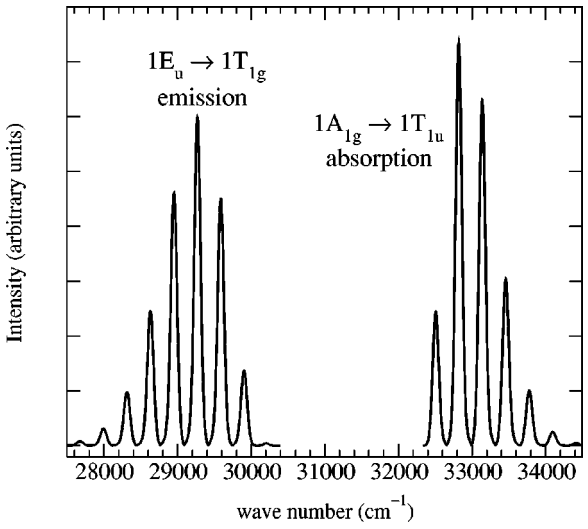

FIG. 3. Calculated intensity profile of the electric dipole allowed absorption $1\,A_{1g}\rightarrow1\,T_{1u}$ and emission $1\,E_u\rightarrow1\,T_{1g}$ bands in $Cs_2ZrCl_6:U^{4+}$. See text for details.

the $1A_{1g}$ ground state. Furthermore, an almost negligible intensity is predicted for the 0–0 line of the $1E_u \rightarrow 1T_{1g}$ emission (Fig. 3).

We would like to compare our results with those of a very recent, well-resolved, high-resolution emission spectrum of isoelectronic $4f^2$ Pr^{3+} ion doped in Cs_2NaYCl_6 cubic elpasolite reported by Tanner *et al.*[57] They identify all the observed (dipole allowed) zero phonon lines on the assumption that the symmetry of the lowest $4f^15d(t_{2g})^1$ state is E_u: The highest energy zero phonon line measured at 38 772 cm^{-1}, has been assigned as the $1E_u \rightarrow 1T_{1g}$ emission and the rest of transitions have been identified as emissions from $1E_u$ to several higher $4f^2$ crystal levels. Our results in U^{4+}-doped Cs_2ZrCl_6 show that the symmetry of the lowest $5f^16d(t_{2g})^1$ state is E_u. This supports the assumption of Tanner *et al.*[57] Here, the $1E_u \rightarrow 1T_{1g}$ zero phonon line is calculated to be 30 234 cm^{-1} (cf. Table III), some 8500 cm^{-1} lower in energy than that of $Cs_2NaYCl_6:Pr^{3+}$. This lowering from Pr^{3+} to U^{4+} is comparable to that observed in the lowest $f^1 \rightarrow d^1$ transition in isoelectronic $4f^1$ $Cs_2NaYCl_6:Ce^{3+}$ and $5f^1$ $Cs_2ZrCl_6:Pa^{4+}$ materials: 8196 cm^{-1}.[20,58,59]

We cannot ascertain the accuracy of the energies of the $5f^16d^1$ levels directly, given that experimental data are not available for the $Cs_2ZrCl_6:U^{4+}$ crystal; we can only estimate it by comparing with the results of analogous calculations. In effect, spin–orbit CI AIMP embedded cluster calculations[17] have been recently done on $Cs_2ZrCl_6:(PaCl_6)^{2-}$ which have been compared to available experimental data.[20,58] The two lowest $5f^1 \rightarrow 6d(t_{2g})^1$ transition energies have been found to be low by some 1700 cm^{-1} compared to experiment. However, the basis sets and the methods we use here to treat electron correlation are expected to be more accurate, so that smaller errors should be expected in the results of this work. In particular, in $Cs_2NaYCl_6:U^{3+}$, using the same basis sets and methods we use here, the discrepacies between the calculated energy of the lowest $5f^3-5f^26d(t_{2g})^1$ electronic origins and their measured values[60] are smaller than 1000 cm^{-1}.[19]

In order to help to understand the structure of the $5f^16d^1$ manifold, in Fig. 6 in the Supplementary Material Section of Ref. 43, we present a correlation diagram between the levels of the $5f^16d(t_{2g})^1$ and $5f^16d(e_g)^1$ manifolds of $Cs_2ZrCl_6:(UCl_6)^{2-}$ and the 1-open shell electron levels of $Cs_2ZrCl_6:(PaCl_6)^{2-}$. It shows the correlation between the irreducible representations of the one electron levels and their two-electron products. Only the correlations with the lowest and highest one-electron states are indicated in the diagram for the $5f^16d(t_{2g})^1$ manifold, for clarity: $5f^1(\Gamma_{7u},\Gamma_{8u}) \times 6d(t_{2g})^1(\Gamma_{8g})$ leading to $1E_u-3T_{1u}$, and $5f^1(\Gamma_{6u}) \times 6d(t_{2g})^1(\Gamma_{8g},\Gamma_{7g})$ to $9T_{2u}-11T_{1u}$. Similarly, the lowest $11T_{2u}-14T_{1u}$ and highest $10E_u-18T_{1u}$ states of the $5f^16d(e_g)^1$ manifold can be correlated with $5f^1(\Gamma_{7u},\Gamma_{8u}) \times 6d(e_g)^1(\Gamma'_{8g})$ and $5f^1(\Gamma'_{7u},\Gamma'_{8u},\Gamma_{6u}) \times 6d(e_g)^1(\Gamma'_{8g})$ couplings (where Bethe's notation has been used for the one-electron Kramer's doublets).

V. UPCONVERSION MECHANISM IN $Cs_2ZrCl_6:U^{4+}$

As mentioned in the Introduction, different interpretations have been given to the observed green to blue upconversion luminescence of $Cs_2ZrCl_6:U^{4+}$ samples at room temperature, which associate the emission with either U^{4+} or UO_2^{2+} luminescent impurities. The points we stress and discuss here are the following: (i) Whatever the luminescent impurity is: U^{4+} or UO_2^{2+}, it has to be pumped to energy levels higher than 19 436 cm^{-1}, the energy of the incident photons, and (ii) possible pumping mechanisms for U^{4+} and UO_2^{2+} exist which involve energy levels of the $5f^16d(t_{2g})^1$ manifold of U^{4+} and, therefore, efficient electric dipole allowed $5f^2-f^16d(t_{2g})^1$ transitions. In what follows we briefly describe the common observations in the first place; then, we summarize the pumping mechanisms which have been suggested by each group and we include the mechanisms that can be considered if the $5f^16d(t_{2g})^1$ levels are taken into account (which are compatible with the observations and with the spectroscopic data available for both $Cs_2ZrCl_6:U^{4+}$ and $Cs_2ZrCl_6:UO_2^{2+}$ materials).

Both Xu *et al.*[6] and Tanner *et al.*[12] have experimentally observed that green laser (19 436 cm^{-1}) excitation of U^{4+}-doped Cs_2ZrCl_6 crystals is followed by the emission of higher energy photons at room temperature. In particular, five band centers at 19 780, 20 010, 20 280, 20 700, and 20 970 cm^{-1} have been reported by Xu *et al.*,[6,61] which have also been observed by Tanner *et al.*,[12] together with a total of eleven emission lines between 19589 and 20 982 cm^{-1}.[12] The variation of the relative intensity of the blue emission lines as temperature is lowered to 200 K has been studied by Xu *et al.*[61] using the same 19 436 cm^{-1} excitation; they have shown that the intensity of the 19 780, 20 010, 20 280 cm^{-1} bands is higher at 200 K than at 300 K, whereas the intensity of the 20 700 and 20 970 cm^{-1} bands decreases to the point that they are not observed at 200 K.[61] The emission spectrum of UO_2^{2+}-doped Cs_2ZrCl_6 crystals upon 19 436 cm^{-1} excitation has not been reported, to our knowledge.

In the upconversion mechanism proposed by Xu *et al.*[6] the pumping occurs through a two-photon absorption of the U^{4+} ions: A first green photon (19 436 cm^{-1}) is expected to excite the sample into the $^3P_1$ level,[6] which corresponds to $8T_{1g}$ (at 18 871 cm^{-1}, see Table IV); nonradiative decay is expected to follow from $8T_{1g}(^3P_1)$ to the lowest level associated with $^3F_2$, that is the $2E_g(^3F_2)$ state, from where the second green photon is absorbed to end in a virtual unassigned level. If the experimental values of the energy levels listed in Table IV are used, the energy of the final state of the $2E_g(^3F_2)$ excited state absorption would be around 24 500 cm^{-1}, which suggests that the $5f^2$ low-spin $9E_g$ state might be reached through a low intensity, hot vibronic absorption. Nonradiative decay down to the emitting $5f^2$ levels of U^{4+} would follow.[6]

On the other hand, according to Tanner *et al.*,[12] the blue emission is due to UO_2^{2+} and the pumping of the eleven levels whose energies (19 589–20 982 cm^{-1}) are higher than the green 19 436 cm^{-1} photons is explained differently: The authors state that the anti-Stokes emission is not due to upconversion but to absorption of the incident photons by

thermally populated vibronic states of UO_2^{2+}.[12] However, the lowest electronic origin of UO_2^{2+} ion doped in the Cs_2ZrCl_6 host (where it creates D_{4h} $UO_2Cl_4^{2-}$ defect clusters), associated with the $A_{1g}\leftrightarrow E_g$ transition has been measured in low-temperature, high-resolution luminescence spectra using 21 470 cm^{-1} excitation and it has been found to be at 19 692 cm^{-1} at 20 K.[62] Its position has been shown to shift to higher energy values with temperature; this shift being about 10 cm^{-1} as temperature is increased from 20 to 125 K.[62] The lowest values of the ungerade vibrational frequencies for the ground state of the $UO_2Cl_4^{2-}$ defects deduced from the low-temperature luminescence spectra are: 116 (O–U–Cl out of plane bend) and 247 cm^{-1} (O–U–O bend).[62] Thus the corresponding hot vibronic absorptions from the A_{1g} ground state would lie at 19 576–19 586 and 19 445–19 455 cm^{-1} if the 20–125 K values of the zero-phonon transition are used. All these data indicate that the 19 436 cm^{-1} laser cannot be expected to excite directly the uranyl ions at 300 K, and make it reasonable to search for alternative pumping mechanisms which enable the blue UO_2^{2+} emission upon 19 436 cm^{-1} excitation.

Let us now discuss how the pumping of either U^{4+} or UO_2^{2+} ions could occur, taking into account the experimental energy levels known for the $Cs_2ZrCl_6:U^{4+}$, $Cs_2ZrCl_6:UO_2^{2+}$, and $Cs_2UO_2Cl_4$ crystals and the energies of the $Cs_2ZrCl_6:U^{4+}$ $5f^16d^1$ levels obtained in this work.

As suggested by Xu *et al.*,[6] the first 19 436 cm^{-1} green photon excites the U^{4+} impurity ions to their $5f^2$ 8 $T_{1g}(^3P_1)$ level (note that 6 A_{1g} and 9 T_{1g} states should be some 78 and 459 cm^{-1} above, according to our calculations, and could also be excited). The notable low-spin character (Table III) of the states in the 8 T_{2g}–9 T_{2g} group, which lie below the excited 8 T_{1g} level, together with the significant 1645 cm^{-1} energy gap with the set of levels lying further below, commented in Sec. IV B (Table IV), makes it reasonable to expect that some of them could be stable enough so as to be capable of producing the second green excited state absorption (ESA). If the experimental values of the energy levels listed in Table IV are used, the final states corresponding to the ESA from the 8 T_{2g}–9 T_{2g} group and from 8 T_{1g} lie at around 34 100–36 300, and 38 300 cm^{-1}, respectively, which means that the $5f^16d(t_{2g})^1$ manifold would be reached in an energy region where electronic states of different spatial symmetry and total spin-triplet character occur (see Table IV). This is so, even if the errors of the calculated energy values were those estimated in Sec. IV C. This type of ESA is very different from that proposed by Xu *et al.*,[6] since the latter corresponds to a $5f^2\rightarrow 5f^2$ dipole forbidden (and largely spin-forbidden) absorption whereas the former corresponds to a more efficient $5f^2\rightarrow 5f^16d(t_{2g})^1$ dipole allowed broad absorption. The proposed two-photon absorption is schematically illustrated in Fig. 4. From the $5f^16d(t_{2g})^1$ states nonradiative relaxation could occur down to the $5f^2$ manifold as indicated in Fig. 4, this enabling $5f^2\rightarrow 5f^2$ U^{4+}-doped emission spectrum in the blue (upconversion), green, and red, as described by Xu *et al.*[6]

Alternatively, the excitation of the U^{4+} ions into their $5f^16d(t_{2g})^1$ states described above could be followed by energy transfer to the UO_2^{2+} impurities, in analogy to what has been observed in Pr^{3+} and Ce^{3+} co-doped Cs_2NaYCl_6,[22] which would be responsible for the blue emission as stated by Tanner *et al.*[12] In effect, violet and ultraviolet (UV) $4f5d\rightarrow 4f^2$ and $5d\rightarrow 4f$ emission spectra of isoelectronic Pr^{3+} and of Ce^{3+} co-doped ions in Cs_2NaYCl_6 have been recently measured at room temperature and 77 K after Pr^{3+} blue (487 nm=20 503 cm^{-1}) excitation.[22] The UV upconversion emission of the Pr^{3+} ions has been interpreted as resulting from a two-photon absorption process very similar to the one proposed here, where the first blue photon populates the $^3P_{0,1,2}$, $^1I_6$ levels of Pr^{3+} and the second one produces a strong dipole allowed $^3P_0\rightarrow 4f^15d^1$ ESA which populates the $4f^15d^1$ states and leads to $4f^15d^1$ emissions to different $4f^2$ levels. The blue to violet+UV upconversion emission of the Ce^{3+} ions, which do not have energy levels coinciding with the blue exciting light, has been interpreted to occur as a consequence of energy transfer from the $4f5d$ excited Pr^{3+} ions to the Ce^{3+} co-doped ions. This latter mechanism, could, in principle, also occur in U^{4+}-doped Cs_2ZrCl_6 crystals contaminated (or co-doped) with UO_2^{2+} impurities. For this energy transfer to occur,[22] the U^{4+} $5f^16d(t_{2g})^1\rightarrow 5f^2$ bands should overlap to a certain extent UO_2^{2+} ground-state absorption bands. In conection with this, it has been shown that the $A_{1g}\rightarrow E_g$ electronic origin of the $UO_2Cl_4^{2-}$ defect in Cs_2ZrCl_6 crystal appears at some 400 cm^{-1} lower energy than the corresponding (D_{2h}) $A_g\rightarrow B_{2g},B_{3g}$ zero-phonons in neat $Cs_2UO_2Cl_4$ crystals, a shift which has been associated with the different crystal environments of the $UO_2Cl_4^{2-}$ units.[62] Therefore, the location of the absorption bands of $Cs_2UO_2Cl_4$ crystals, which have been measured through one- and two-photon absorption spectroscopy by Denning and co-workers,[63,64] can give a fairly good idea of possible pumping bands of uranyl in Cs_2ZrCl_6, and, ultimately, of their overlap with $5f^16d(t_{2g})^1\rightarrow 5f^2$ U^{4+} emission bands. Absorption bands corresponding to twelve electronic origins were observed in $Cs_2UO_2Cl_4$ crystals in the 20 000–28 000 cm^{-1} spectral range through one- and two-photon spectroscopy, and in the 28 000–32 000 cm^{-1} interval through two-photon spec-

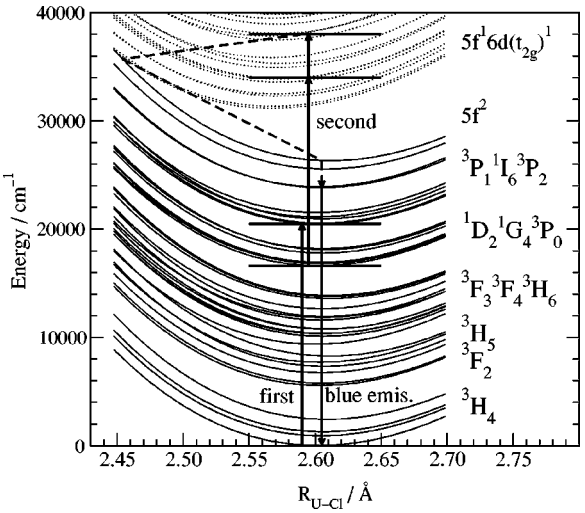

FIG. 4. Green to blue upconversion mechanism proposed for $Cs_2ZrCl_6:U^{4+}$.

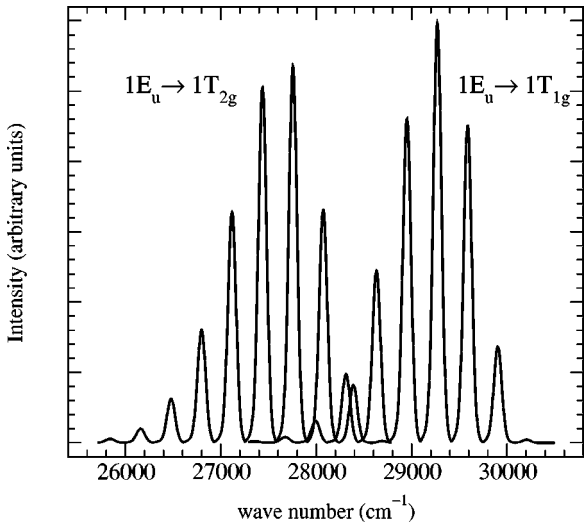

FIG. 5. Calculated intensity profile of the electric dipole allowed $5f^16d(t_{2g})^1\ 1E_u \rightarrow 5f^2\ 1T_{1g}$, $1T_{2g}$ emission bands in $Cs_2ZrCl_6:U^{4+}$.

troscopy.[63,64] In Fig. 5 we show the intensity profiles of the two highest electric dipole allowed emissions: $1E_u \rightarrow 1T_{1g}$, $1T_{2g}$, connecting the $5f^16d(t_{2g})^1\ 1E_u$ excited state with two crystal components of the $U^{4+}\ ^3H_4$. (Note that the relative intensities of the two $1E_u \rightarrow 5f^2$ bands in Fig. 5 are arbitrary.) The overlap between the $1E_u \rightarrow 5f^2$ U^{4+} bands shown in Fig. 5 and the ground state absorption bands that can be expected for UO_2^{2+} is apparent, which indicates that the $U^{4+} \rightarrow UO_2^{2+}$ energy transfer can occur via intermediate $5f^16d(t_{2g})^1$ states, this being a plausible mechanism to explain the green to blue upconversion of uranyl impurities in $Cs_2ZrCl_6:U^{4+}$ materials contaminated or co-doped with UO_2^{2+} ions.

VI. CONCLUSIONS

In this paper we have applied the *ab initio* model potential embedded cluster method (AIMP) to the calculation of the U–Cl equilibrium distances, totally symmetric vibrational frequencies, and $5f^2 \rightarrow 5f^2$, $5f^2 \rightarrow 5f^16d^1$ electronic transitions of the octahedral $(UCl_6)^{2-}$ defect cluster in the Cs_2ZrCl_6 host crystal. The Cs_2ZrCl_6 AIMP embedding potential produced in previous works incorporates quantum-mechanical host effects. The Cowan–Griffin AIMP and the multistate second-order multiconfigurational perturbation (MS-CASPT2) methods allow to account for spin-free relativistic effects and correlation of 58 $(UCl_6)^{2-}$ valence electrons, respectively. These effects are incorporated in a final set of spin–orbit configuration interaction (CI) calculations by means of the spin-free state shifted (sfss) Wood–Boring AIMP Hamiltonian. We have calculated the $5f^2-5f^2$ spectrum of U^{4+} in gas phase and we have compared our results with experiments and with previous relativistic Dirac–Coulomb coupled cluster calculations to check the quality of the methods used at the atomic level; the root-mean square (rms) deviation of the $5f^2-5f^2$ transition energies relative to available experimental data is 214 cm^{-1}. The results of the spin–orbit CI calculations on the $Cs_2ZrCl_6:(UCl_6)^{2-}$ system show that the 98 spin–orbit levels can be grouped in three superconfigurations: $5f^2$, $5f^16d(t_{2g})^1$, and $5f^16d(e_g)^1$; their calculated U–Cl equilibrium distances and totally symetric vibrational frequencies are extremely close within each superconfiguration and are: $5f^2$ [$R_e = 2.605 \pm 0.003$ Å, $\overline{\nu}_{a_{1g}} = 320 \pm 2\ cm^{-1}$], $5f^16d(t_{2g})^1$ [$R_e = 2.571 \pm 0.004$ Å, $\overline{\nu}_{a_{1g}} = 324 \pm 1\ cm^{-1}$], and $5f^16d(e_g)^1$ [$R_e = 2.642 \pm 0.004$ Å, $\overline{\nu}_{a_{1g}} = 299 \pm 3\ cm^{-1}$]. The rms deviations of the $5f^2 \rightarrow 5f^2$ transition energies of $Cs_2ZrCl_6:(UCl_6)^{2-}$ relative to experimental data grow with energy as follows: $1A_{1g}-1T_{2g}$: 24, $2E_g-3E_g$: 432, $2A_{1g}-7T_{2g}$: 719, $8T_{2g}-9T_{2g}$: 1459, and $8T_{1g}-9E_g$: 1691 cm^{-1}. The energies of the crystal levels of the $5f^16d(t_{2g})^1$ and $5f^16d(e_g)^1$ manifolds are predicted to be 31 100–51 000 and 67 300–85 500 cm^{-1} above the ground state, respectively. Our results show a large energy gap of 23 00 cm^{-1} between the lowest electric dipole allowed zero-phonon absorption from the $5f^2$ ground state, $1A_{1g} \rightarrow 1T_{1u}$ (32 500 cm^{-1}), and the highest electric dipole allowed zero-phonon emission from the first $5f^16d(t_{2g})^1$ excited state, which is found to be $1E_u \rightarrow 1T_{1g}$ (30 200 cm^{-1}). Both transitions should be observable before the strong absorption of the host. The results of our calculations give new insight into the discussion on the green to blue upconversion of U^{4+}-doped Cs_2ZrCl_6. They suggest that $5f^16d^1$ excited electronic states of the embedded $(UCl_6)^{2-}$ cluster are involved in the upconversion mechanism irrespective of which impurity is the luminescent center: U^{4+} or UO_2^{2+} in contaminated samples.

ACKNOWLEDGMENTS

This work was partly supported by grants from Ministerio de Ciencia y Tecnología, Spain (Dirección General de Investigación, PB98-0108 and BQU2002-01316).

[1] M. Wermuth and H. U. Güdel, J. Am. Chem. Soc. **121**, 10 102 (1999).
[2] R. Valiente, O. S. Wenger, and H. U. Güdel, Phys. Rev. B **63**, 165 102 (2001).
[3] C. D. Flint and P. A. Tanner, Mol. Phys. **53**, 429 (1984).
[4] S. Hubert, C. Li Song, M. Genet, and F. Auzel, J. Solid State Chem. **61**, 252 (1986).
[5] N. A. Stump, G. M. Murray, G. D. Del Cul, R. G. Haire, and J. R. Peterson, Radiochim. Acta **54**, 129 (1993).
[6] W. Xu, S. Dai, L. M. Toth, and J. R. Peterson, Chem. Phys. **193**, 339 (1995).
[7] K. M. Murdoch, R. Cavellec, E. Simoni, M. Karbowiak, S. Hubert, M. Illemassene, and N. M. Edelstein, J. Chem. Phys. **108**, 6353 (1998).
[8] P. J. Deren, W. Strek, E. Zych, and J. Drozdzynski, Chem. Phys. Lett. **332**, 308 (2000).
[9] M. Illemassene, N. M. Edelstein, K. M. Murdoch, M. Karbowiak, R. Cavellec, and S. Hubert, J. Lumin. **86**, 45 (2000).
[10] J. C. Wright, in *Radiationless Processes in Molecules and Condensed Phases*, edited by F. K. Fong (Springer, Berlin, 1976), pp. 239–295.
[11] N. Yu. Kirikova, M. Kirm, J. C. Krupa, V. N. Makhov, G. Zimmerer, and J. Y. Gesland, J. Lumin. **97**, 174 (2002).
[12] P. A. Tanner, J. Dexpert-Ghys, Z. W. Pei, and J. Lin, Chem. Phys. **215**, 125 (1997).
[13] R. A. Satten, C. L. Schreiber, and E. Y. Wong, J. Chem. Phys. **42**, 162 (1965).
[14] C. D. Flint and P. A. Tanner, Mol. Phys. **61**, 389 (1987).
[15] L. Seijo and Z. Barandiarán, in *Computational Chemistry: Reviews of Current Trends*, edited by J. Leszczynski (World Scientific, Singapore, 1999), Vol. 4, p. 55.
[16] Z. Barandiarán and L. Seijo, J. Chem. Phys. **89**, 5739 (1988).
[17] L. Seijo and Z. Barandiarán, J. Chem. Phys. **115**, 5554 (2001).

[18] L. Seijo, Z. Barandiarán, and B. Ordejón, Mol. Phys. **101**, 73 (2003).
[19] L. Seijo and Z. Barandiarán, J. Chem. Phys. **118**, 5335 (2003).
[20] N. Edelstein, W. K. Kot, and J. C. Krupa, J. Chem. Phys. **96**, 1 (1992).
[21] C. D. Flint and P. A. Tanner, Mol. Phys. **53**, 437 (1984).
[22] M. Laroche, M. Bettinelli, S. Girard, and R. Moncorgé, Chem. Phys. Lett. **311**, 167 (1999).
[23] L. Seijo and Z. Barandiarán, J. Chem. Phys. **118**, 1921 (2003).
[24] Detailed core and embedding AIMP data libraries in electronic format are available from the authors upon request or directly at the address http://www.uam.es/quimica/aimp/-Data/AIMPLibs.html. See also Ref. 40.
[25] R. Llusar, M. Casarrubios, Z. Barandiarán, and L. Seijo, J. Chem. Phys. **105**, 5321 (1996).
[26] L. Seijo and Z. Barandiarán (unpublished).
[27] K. Andersson, P.-Å. Malmqvist, B. O. Roos, A. J. Sadlej, and K. Wolinski, J. Phys. Chem. **94**, 5483 (1990).
[28] K. Andersson, P.-Å. Malmqvist, and B. O. Roos, J. Chem. Phys. **96**, 1218 (1992).
[29] J. Finley, P.-Å. Malmqvist, B. O. Roos, and L. Serrano-Andrés, Chem. Phys. Lett. **288**, 299 (1998).
[30] A. Zaitsevskii and J. P. Malrieu, Chem. Phys. Lett. **233**, 597 (1995).
[31] B. O. Roos, P. R. Taylor, and P. E. M. Siegbahn, Chem. Phys. **48**, 157 (1980); P. E. M. Siegbahn, A. Heiberg, J. Almlöf, and B. O. Roos, J. Chem. Phys. **74**, 2384 (1981); P. Siegbahn, A. Heiberg, B. Roos, and B. Levy, Phys. Scr. **21**, 323 (1980).
[32] L. Seijo, Z. Barandiarán, and E. Harguindey, J. Chem. Phys. **114**, 118 (2001).
[33] R. D. Cowan and D. C. Griffin, J. Opt. Soc. Am. **66**, 1010 (1976).
[34] J. H. Wood and A. M. Boring, Phys. Rev. B **18**, 2701 (1978).
[35] M. Dolg and H. Stoll, in *Electronic Structure Calculations for Molecules Containing Lanthanide Atoms*, *Vol. 22 of Handbook on the Physics and Chemistry of Rare Earths*, edited by K. A. Gschneider, Jr. and L. Eyring (Elsevier, Amsterdam, 1995), p. 1.
[36] L. Seijo, J. Chem. Phys. **102**, 8078 (1995).
[37] Z. Barandiarán and L. Seijo, Can. J. Chem. **70**, 409 (1992).
[38] T. H. Dunning and P. J. Hay, in *Modern Theoretical Chemistry*, edited by H. F. Schaefer III (Plenum, New York, 1977).
[39] J. Andzelm, M. Klobukowski, E. Radzio-Andzelm, Y. Sakai, and H. Tatewaki, *Gaussian Basis Sets for Molecular Calculations*, edited by S. Huzinaga (Elsevier, Amsterdam, 1984).
[40] MOLCAS version 5, K. Andersson, M. Barysz, A. Bernhardsson *et al.*, Lund University, Sweden, 2000.
[41] R. M. Pitzer and N. W. Winter, J. Phys. Chem. **92**, 3061 (1988).
[42] COLUMBUS suite of programs. (ARGOS, CNVRT, SCFPQ, LSTRN, CGDBG, and CIDBG) R. M. Pitzer (principal author). See A. H. H. Chang and R. M. Pitzer, J. Am. Chem. Soc. **111**, 2500 (1989), and references therein for a description. CNVRT and LSTRN have been adapted to handle AIMP integrals by L. Seijo. CIDBG has been modified for spin-free-state-shifted spin–orbit CI calculations by M. Casarrubios.
[43] See EPAPS Document No. E-JCPSA6-118-304316 for data and results of AIMP embedded cluster calculations on $Cs_2ZrCl_6:U^{4+}$. A direct link to this document may be found in the online article's HTML reference section. The document may also be reached via the EPAPS homepage (http://www.aip.org/pubservs/epaps.html) or from ftp.aip.org in the directory /epaps/. See the EPAPS homepage for more information.
[44] J. F. Wyart, V. Kaufman, and J. Sugar, Phys. Scr. **22**, 389 (1980).
[45] C. H. H. Van Deurzen, K. Rajnak, and J. G. Conway, J. Opt. Soc. Am. B **1**, 45 (1984).
[46] E. Eliav, U. Kaldor, and Y. Ishikawa, Phys. Rev. A **51**, 225 (1995).
[47] R. W. Field, Ber. Bunsenges. Phys. Chem. **86**, 771 (1982).
[48] I. Gotkis, J. Phys. Chem. **95**, 6086 (1991).
[49] S. Sugano, Y. Tanabe, and H. Kamimura, *Multiplets of Transition—Metal Ions in Crystal* (Academic, New York, 1970).
[50] S. Siegel, Acta Crystallogr. **9**, 827 (1956).
[51] S. A. Pollack and R. A. Satten, J. Chem. Phys. **36**, 804 (1962).
[52] D. Johnston, R. Satten, and E. Wong, J. Chem. Phys. **44**, 687 (1966).
[53] D. R. Johnston, R. A. Satten, C. L. Shreiber, and E. Y. Wong, J. Chem. Phys. **44**, 3141 (1966).
[54] R. A. Satten, C. L. Schreiber, and E. Y. Wong, J. Chem. Phys. **78**, 79 (1983).
[55] E. J. Heller, J. Chem. Phys. **62**, 1544 (1975).
[56] E. J. Heller, Acc. Chem. Res. **14**, 368 (1981).
[57] P. A. Tanner, C. S. K. Mak, and M. D. Faucher, Chem. Phys. Lett. **343**, 309 (2001).
[58] D. Piehler, W. K. Kot, and N. Edelstein, J. Chem. Phys. **94**, 942 (1991).
[59] R. W. Schwartz and P. N. Schatz, Phys. Rev. B **8**, 3229 (1973).
[60] M. Karbowiak, J. Drozdzynski, S. Hubert, E. Simoni, and W. Strek, J. Chem. Phys. **108**, 10181 (1998).
[61] W. Xu, S. Dai, L. M. Toth, G. D. Del Cul, and J. R. Peterson, J. Solid State Chem. **116**, 113 (1995).
[62] D. H. Metcalf, S. Dai, G. D. Del Cul, and L. M. Toth, Inorg. Chem. **34**, 5573 (1995).
[63] R. G. Denning, T. R. Snellgrove, and D. R. Woodwark, Mol. Phys. **30**, 1819 (1975).
[64] T. J. Barker, R. G. Denning, and J. R. G. Thorne, Inorg. Chem. **26**, 1721 (1987).